

DENSITY ESTIMATION IN LARGE-SCALE WIRELESS SENSOR NETWORKS

A THESIS SUBMITTED TO
THE GRADUATE SCHOOL OF NATURAL AND APPLIED SCIENCES
OF
MIDDLE EAST TECHNICAL UNIVERSITY

BY

ALPEREN EROĞLU

IN PARTIAL FULFILLMENT OF THE REQUIREMENTS
FOR
THE DEGREE OF MASTER OF SCIENCE
IN
COMPUTER ENGINEERING

JANUARY 2015

Approval of the thesis:

DENSITY ESTIMATION IN LARGE-SCALE WIRELESS SENSOR NETWORKS

submitted by **ALPEREN EROĞLU** in partial fulfillment of the requirements for the degree of **Master of Science in Computer Engineering Department, Middle East Technical University** by,

Prof. Dr. Gülbin Dural Ünver
Dean, Graduate School of **Natural and Applied Sciences**

Prof. Dr. Adnan Yazıcı
Head of Department, **Computer Engineering**

Assoc. Prof. Dr. Ertan Onur
Supervisor, **Computer Engineering Department, METU**

Assoc. Prof. Dr. Halit Oğuztüzün
Co-supervisor, **Computer Engineering Department, METU**

Examining Committee Members:

Prof. Dr. Ahmet Coşar
Computer Engineering Department, METU

Assoc. Prof. Dr. Ertan Onur
Computer Engineering Department, METU

Assoc. Prof. Dr. Halit Oğuztüzün
Computer Engineering Department, METU

Dr. Cevat Şener
Computer Engineering Department, METU

Selami Çiftçi, M.Sc.
Team Leader, Argela Technologies

Date:

I hereby declare that all information in this document has been obtained and presented in accordance with academic rules and ethical conduct. I also declare that, as required by these rules and conduct, I have fully cited and referenced all material and results that are not original to this work.

Name, Last Name: ALPEREN EROĞLU

Signature :

ABSTRACT

DENSITY ESTIMATION IN LARGE-SCALE WIRELESS SENSOR NETWORKS

Erođlu, Alperen

M.S., Department of Computer Engineering

Supervisor : Assoc. Prof. Dr. Ertan Onur

Co-Supervisor : Assoc. Prof. Dr. Halit Ođuztüzün

January 2015, 60 pages

Density estimation is a significant problem in large-scale wireless ad-hoc networks since the density drastically impacts the network performance. It is crucial to make the network adaptive in the run-time to the density changes that may not be predictable in advance. Local density estimators are required while taking run-time control decisions to improve the network performance. A wireless node may estimate the density locally by measuring the received signal strength (RSS) of packets sent by its neighbours. In this thesis, RSS-based individual and cooperative density estimators are validated by controlled field experiments conducted in the FIT IoT-LAB test-bed, in France. According to the experiments these methods cannot be used as accurate density estimators in practice. The success of the individual density is significantly affected by the position of the estimating node and the number of its neighbours. Also, the cooperative density estimator is affected negatively by correlated data. Hence, a new fusion approach is proposed as a new density estimator. New method is more accurate than the two other density estimators. However, it should be considered that the RSS is prone to large- and small-scale fading, and this phenomenon negatively affects the accuracy of density estimators.

Keywords: Density Estimation, Received Signal Strength, RSS, Path-loss Exponent Estimation, Real Test-bed, Large-scale Wireless Sensor Network

ÖZ

GENİŞ ÖLÇEKLİ ALGILAYICI AĞLARINDA YOĞUNLUK TAHMİNİ

Erođlu, Alperen

Yüksek Lisans, Bilgisayar Mühendisliđi Bölümü

Tez Yöneticisi : Doç. Dr. Ertan Onur

Ortak Tez Yöneticisi : Doç. Dr. Halit Ođuztüzün

Ocak 2015 , 60 sayfa

Yođunluk, ađ performansını büyük ölçüde etkilediđinden geniş ölçekli kablosuz ađlardaki yođunluk kestirimi önemli bir problemdir. Önceden tahmin edilemeyen yođunluk deđişikliklerine, çalışma zamanında ađın uyum sağlaması önemlidir. Çalışma zamanı kontrol kararları ve ađ performansını artırmak için bölgesel yođunluk kestirimi gereklidir. Bir algılayıcı komşularının göndermiş olduđu paketlerin sinyal gücü deđerlerini kullanarak bölgesel yođunluk kestirimi yapabilir. Bu tezde sinyal gücü deđerini kullanan iki adet yođunluk kestirimi uygulaması, bireysel ve işbirlikli yođunluk kestirimi, kontrollü alan deneyleri ile Fransa'da yer alan IoT-Lab algılayıcı ađında deđerlendirilmiştir. Sonuçlara göre bireysel yođunluk kestirimi ve işbirlikli yođunluk kestirimi metodları pratikte verimli yođunluk tahmincisi olarak kullanılabilirler. Bireysel yođunluk tahmincisinin başarısı tahminci düđümün bulunduđu yerden ve komşularının sayılarından büyük ölçüde etkilenmektedir. Diđeri ise korele verilerden etkilenmektedir. Bu çalışmada daha başarılı sonuçlar veren ve bu iki tahmincinin birleştirilmesinden oluşan yeni bir yaklaşım önerilmiştir. Bu çalışmanın sonuçları sinyal gücünün geniş ve küçük ölçekli zayıflamaya maruz kalması nedeniyle yođunluk kestiriminin dođruluđunu olumsuz şekilde etkilediđini göstermektedir.

Anahtar Kelimeler: Yođunluk Tahmini, Sinyal Gücü, Yol Kayıp Deđer Tahmini , Gerçek Sınama ortamı, Geniş Ölçekli Ađlar

I dedicate this thesis to my grandfather Mehmet EROĞLU. Despite him not being with us, I believe that he is very glad as always because of my success. I also dedicate this thesis to My Family. Endless thanks to my family

ACKNOWLEDGMENTS

First of all, I would like to express my sincere gratitude to my supervisor Assoc. Prof. Dr. Ertan ONUR for the continuous support of my M.Sc. thesis and research at the Department of Computer Engineering in Middle East Technical University (METU), for his great patience, motivation, enthusiasm, friendship, and immense knowledge. His guidance helped me in all the time of research and writing of this thesis. I could not have imagined having a better advisor and mentor for my M.Sc. thesis.

I would like to express my special thanks to my co-advisor Assoc. Prof. Dr. Halit OĞUZTÜZÜN for his continuous assistance and precious guidance since I started to the graduate school at the Department of Computer Engineering in METU. In addition, thanks to him for his contributions and revisions regarded with my thesis.

I would also like to thank the committee members of my M.Sc. thesis, Prof. Dr. Ahmet COŞAR, Dr. Cevat ŞENER, and Selami ÇİFTÇİ for their precious discussions and suggestions about my thesis.

I would like to thank to Prof. Dr. Ali H. DOĞRU at Department of Computer Engineering, and Assist. Prof. Dr. Onur PEKCAN at Department of Civil Engineering in Middle East Technical University for their continuous interest and encouragement in my researches. Moreover I also would like to thank to Assist. Prof. Dr. Selim TEMİZER at the Department of Computer Engineering in Middle East Technical University for his guidance related to taking the graduate courses and our own research studies and papers with him in robotic field.

My special thanks to FIT/IoT-Lab, in France and their members for giving us the opportunity to use their test-beds for our experiments during the thesis. They make the usage of platform easier by providing useful documents such as tutorials, and useful scripts. We can easily access the mail archive, this support is also great chance while solving and understanding the problems regarded with our experiments. Moreover, special thanks to IoT-Lab users and administrators for quickly and patiently replying the questions about our experiments.

Sincere thanks to all my friends especially M. Çağrı KAYA, M. Akif AKKUŞ, Mahdi Saedi NIKOO, Hüsnü YILDIZ, Serdar ÇİFTÇİ, Özcan DÜLGER, Alev MUTLU, Selma SÜLOĞLU, Emrah KARAHAN, Selçuk S. KIRAT, Çağrı BEKTAŞ, Abdullah B. KAYA, Ali R. YILMAZ, Mustafa YARGI and others for their kindness and moral support during my study. Thanks for their friendship and memories.

I also thank to our staff Sultan ARSLAN, Zafer ŞANAL, Mehmet DEMİRDÖĞEN, Erol ÖZTAŞ, and Özgür ÇETİN at the Department of Computer Engineering for their kindness support.

All my family, my parents, my grandparents, and my brother deserve special mention for their inseparable support and prayers. My Mother Selma EROĞLU and my Father, Mustafa EROĞLU are in the first place who sincerely raised me with their caring and gently love. My Brother, Bahadır A. EROĞLU, always encourages me.

Finally, I would like to thank everybody who was important to the successful realization of this thesis, as well as expressing my apology that I could not mention personally one by one.

TABLE OF CONTENTS

ABSTRACT	v
ÖZ	vi
ACKNOWLEDGMENTS	viii
TABLE OF CONTENTS	x
LIST OF TABLES	xiii
LIST OF FIGURES	xiv
LIST OF ABBREVIATIONS	xvi
LIST OF SYMBOLS	xvii
CHAPTERS	
1 INTRODUCTION	1
1.1 Problem Definition	1
1.2 Motivation	2
1.3 Methodology	6
1.4 Contribution	6
1.5 Outline	7
2 RELATED WORK	9

2.1	Path-Loss Exponent Estimation	9
2.1.1	Free Space Path-Loss Model	10
2.1.2	Empirical Path-Loss Models	10
2.1.2.1	Okumura Model	10
2.1.2.2	Hata Model	11
2.1.2.3	COST 231 Extension to Hata Model Model	12
2.1.2.4	Piecewise Linear Model	12
2.2	Distance Estimation	13
2.2.1	Received Signal Strength Based Distance estimation	13
2.2.2	Time of Arrival (TOA)	13
2.2.3	Time Difference of Arrival (TDOA)	13
2.2.4	Hop Count	14
2.2.5	Comparison of the distance estimation methods . .	14
3	DENSITY ESTIMATION	17
3.1	Density Estimation Methods	17
3.1.1	Individual Density Estimation	18
3.1.2	Cooperative Density Estimation	20
3.2	Path-Loss Exponent Estimation	20
3.2.1	Simplified Path-Loss Model	21
4	EXPERIMENTAL RESULTS	23
4.1	Testbed	23

4.1.1	Deployment	23
4.1.2	Usage of Platform	25
4.2	Data Collection	29
4.2.1	Data Gathering Devices	29
4.2.2	Data Gathering Method	30
4.2.3	Data Manipulation	30
4.2.4	Evaluation of Path-Loss Exponent	37
4.3	Results of Cooperative Density Estimation	38
4.4	Results of Individual Density Estimation	45
4.5	Comparing Individual and Cooperative Density Estimation	51
4.6	Impact of Path-Loss Exponent	51
4.7	A New Method Based on Fusion of the Individual and Co-operative Density Estimators	52
5	CONCLUSION	55
5.1	Conclusion	55
5.2	Future Work	56
	REFERENCES	57

LIST OF TABLES

TABLES

Table 1.1	The qualitative comparison of the impact of the density regime on various network parameters and performance measures.	5
Table 2.1	The Comparison of the Distance Estimation Techniques	15
Table 3.1	Typical Path-Loss Exponents [15]	21
Table 4.1	Unique Distance Values and Their Average RSSs for the First Experiment.	34
Table 4.2	Unique Distance Values and Their Average RSSs for The Second Experiment	35
Table 4.3	Path-Loss Exponent Estimation Results with Different Number of Nodes with 17 dBm Transmission Power.	37
Table 4.4	Changes on Individual and Cooperative Estimators According to Path-loss Exponent	51

LIST OF FIGURES

FIGURES

Figure 2.1 Piecewise Linear Model for Path-Loss	12
Figure 4.1 The Distribution of Whole Nodes in Lille deployment	24
Figure 4.2 Nodes in Lille deployment for the First Experiment	25
Figure 4.3 A Screenshot From The First Experiment	26
Figure 4.4 A Screenshot From The Second Experiment	27
Figure 4.5 m3 Sensor Node	30
Figure 4.6 Train Data in Logarithmic Scale	31
Figure 4.7 Test Data in Logarithmic Scale 1	32
Figure 4.8 Test Data in Logarithmic Scale 2	33
Figure 4.9 Unique Distances in Logarithmic Scale vs Their Average RSS values	36
Figure 4.10 Real Distances vs The Average of Estimated Distances	38
Figure 4.11 Actual Cooperative Density vs. Estimated Cooperative Density Scatter Plot I	39
Figure 4.12 Actual Cooperative Density vs. Estimated Cooperative Density Error Bar I	40
Figure 4.13 Cooperative Density vs. AAPD I	41
Figure 4.14 Actual Cooperative Density vs. Estimated Cooperative Density Scatter Plot II	42
Figure 4.15 Actual Cooperative Density vs. Estimated Cooperative Density Error Bar II	43
Figure 4.16 Cooperative Density vs. AAPD II	44

Figure 4.17 Actual Individual Density vs. Estimated Individual Density Scatter Plot I	45
Figure 4.18 Actual Individual Density vs. Estimated Individual Density Error Bar I	46
Figure 4.19 Individual Density vs. AAPD I	47
Figure 4.20 Actual Individual Density vs. Estimated Individual Density Scatter Plot II	48
Figure 4.21 Actual Individual Density vs. Estimated Individual Density with 95 confidence interval	49
Figure 4.22 Individual Density vs. AAPD	50
Figure 4.23 Actual Fusion Density vs. Estimated Fusion Density Scatter Plot	52
Figure 4.24 Actual Fusion Density vs. Estimated Fusion Density Error Bar	53
Figure 4.25 Fusion Density vs. AAPD	54

LIST OF ABBREVIATIONS

WSN	Wireless Sensor Network
WSNs	Wireless Sensor Networks
RSS	Received Signal Strength
dB	Decibel
dBm	Decibel Milliwatt
mW	Milliwatt
m	meter
MMSE	Minimum Mean-squared Error
AAPD	Average Absolute Percentage Deviation
GPS	Global Positioning System
PLE	Path-loss Exponent Estimation
IoT	Internet of Things
FIT	Future Internet (of Things)
SSH	Secure Shell
CLI	Command Line Tools
CSMA	Carrier Sense Multiple Access
MAC	Medium Access Control
SUI	Stanford University Interim
TOA	Time of Arrival
TDOA	Time Difference of Arrival

LIST OF SYMBOLS

λ	Actual density
$\hat{\lambda}$	Estimated density
γ	Path-loss exponent
σ	Sample variance
c	The speed of light
d_0	Reference distance
d_i	Estimated distance
f	Frequency
K	Free space wave length
k_{th}	Neighbour proximity degree / Connectivity degree
N	The number of samples while calculating the PLE
n	The number of nodes that transmit a packet to the estimating node
P_t	Transmission power
P_r	Received power
$P_{(mW)}$	RSS in milliwatt
$P_{(dBm)}$	RSS in decibell milliwatt
$P_{(dB)}$	RSS in decibell
r_i	The radius
T	The summation of the summation of the connectivity degree

CHAPTER 1

INTRODUCTION

1.1 Problem Definition

Assume an infinite forest where the trees are randomly distributed with a uniform average density of λ per unit area [30]. An statistician wants to estimate the density $\hat{\lambda}$ by using distances [30]. The statistician chooses a random point in the forest. Then he measures the distance r_1 between himself and the nearest tree. Consider that in πr_1^2 , there is only one tree, and the statistician saves the neighbour proximity degree k_{th} as 1, and calculates the area as πr_1^2 , then he selects another random point. The statistician makes these calculations by considering $j = 1, 2, \dots, \infty$ for k_{jth} and their areas πr_j^2 in several random points. After gathering calculations and measurements, when the statistician divides the summation of the neighbour proximity degrees k_{jth} by the summation of the areas πr_j^2 , then the estimated density $\hat{\lambda}$ can be found. This approach is performed as a density estimator in a wireless sensor network in [29].

In an m dimensional space, suppose that there is a large number of deployed wireless sensor nodes. The distances are not known between the sensor nodes. Nodes transmit packets to their neighbours, and they can measure the received signal strength (RSS) of these packets transmitted by their neighbours. The distances are estimated by using the collected RSS values. After estimating the distances, the neighbour proximities and the calculated areas can be found, then the same approach in [30] is applied. In such networks, the number of sensors and the size of the area determines the density [39]. Density is essential for wireless sensor networks (WSNs) in terms of some problems such as localization, energy conservation, sleep scheduling, topology con-

trol, beam-forming, collaborative signal processing or adequate capacity planning. Protocols of WSNs have to adapt their acts to the density since the throughput in sensor network approaches asymptotically to zero as the density increases [16]. The density of the wireless sensor networks affects the efficiency of the networking protocols. Thus, these protocols have to be adaptive to the provisional changes in the density of the network. Estimating the density may make reconfiguration of the protocols adaptable to enhance the performance of the network. In this thesis, density estimation problem in large-scale wireless sensor networks are dealt with as a real life implementation. There are several solutions to the problem of the density estimation, however we focus on received signal strength based density estimation technique proposed in [29] since the method uses only RSS measurements and this technique can be used in local density estimation [29]. There are two proposed methods called individual density estimation and cooperative density estimation in [29]. In this work, it is shown that a wireless node can estimate the network density individually by using local information such as the received power from its neighbours. It is also possible to estimate the density cooperatively which provides a better estimate. These two models need to be validated in a real life implementation. In this thesis, we focus on the validation of these estimators. We also propose a fusion of these two estimators to improve the accuracy.

1.2 Motivation

In recent years, research and various studies on wireless sensor networks (WSN) are carried out along with the development of technology. Wireless sensor networks (WSNs) can be used in many fields such as monitoring, security, disaster management, habitat monitoring and environmental studies [2, 19, 41]. Especially, it can be observed that WSNs have promising developments to provide some opportunities for real-time monitoring in geographical areas which are prone to disasters [35]. Sensors are deployed to collect local data systematically in areas where they are deployed and send them to another place [19]. Sensors can collect many different types of data such as temperature, humidity, smoke, motion, light and sound perception. The data they have collected can be forwarded between themselves or transmitted to a center.

The collected data are analysed and combined, some decisions can be made based on this manipulated data or systems can be controlled [19]. Sensors are deployed over the area as required by events or the systems that should be controlled, monitored and managed.

Design of a sustainable WSN is a difficult issue. Although, sensors are limited in terms of energy, they are expected to work independently for a long time [4]. Supplying a new energy source or battery for sensors in some environments is not sometimes possible, even if it is possible, this directly brings a cost [38]. Sensor networks can be designed in an application-oriented manner unlike other networks, and as mentioned before these networks can be used in many different areas and for different aims with different capacities and sizes [38]. Particularly in recent years, large-scale dense networks are considered as one of the foremost subjects among research studies. There are hundreds and thousands of sensors in such networks [19]. In such large-scale networks some problems may emerge such as network congestion, collisions, low efficiency and low capacity [29, 38]. Such problems can significantly increase the cost of the communication and cause a delay in the collection and transmission of the data [19]. Therefore, especially in these networks some characteristics and specifications such as energy saving, fault tolerance, long network lifetime, efficient algorithms in data collection should be taken into account because of resource limitations [19]. As a higher number of sensors affects the performance of WSN, independent controlling, random participation or separation of the nodes especially in a dynamic network cause a change in density of the nodes, for this reason the network performance is also affected considerably [29]. It can be seen that how the density effects the quality and the performance measures of the network such as network capacity, throughput, connectivity, delay of the signal between the sender and receiver and other factors in Table 1.1. Such problems should be managed in such networks, and this issue has been studied under the topic of density estimation in several studies and various methods have been developed.

Density estimation is very important solution to adequate capacity planning. These networks should be developed in accordance with the unpredictable changes of density. Run-time decisions should be based on the density estimated locally [29]. The protocols in these networks can be adapt their functions and algorithms according to

the density [7, 11, 16, 29] . In this way, the estimation of the density allows restructuring of the network protocols to improve the performance and throughput of the network [38]. The density estimation in WSNs can also be used for obtaining useful information about the distribution of the mobile devices in crowd management or the scope of such a network. For instance, estimating the density of mobile phones in a stadium will assist in determining the required capacity planning by network managers such as deploying additional base stations for providing better quality of service. As another example, a re-placement or set-up in the network is possible after detecting the deficiencies caused by the sensors which have lost their functionalities. In a WSN, the optimization of the transmission power provides a longer network lifetime and maintains the quality of connection [8, 12] . The node density is used while optimizing the transmission power in the network [8, 12]. In National Basketball Association and Major League Baseball events, wireless devices are used for sharing the experiences of the audiences by adding desirable and available services including features such as multiple streaming-video broadcasts, program information, relevant statistical data, instant on-demand replays of videos, audio commentary [3]. The question is regarded with the possibility of such an operational wireless stadium network by considering the technical and financial feasibility of the system. In the case of such a network design, the density of access points, and any other wireless devices should be considered to obtain an efficient deployment strategy [3]. In WSNs, the energy consumption and coverage of the network are the important problems in terms of gaining the efficient energy consumption, maintaining a longer lifetime. Sleep scheduling is important solution to the problem of reducing the energy consumption, while performing this solution, the coverage and the density of the network should be considered [6, 41, 43, 44]. All these examples show that there is a need for accurate estimation of the density, and while doing this, it is important that the density is estimated locally. The common density estimation methods are explained in Chapter 2. In this thesis, one of common methods called received signal strength based density estimation is used by considering the importance of the local estimation solution without using any extra system [27, 29, 48]. There are few research studies in the literature, in this work, it is focused that proposed two analytic models by [29], and this work had to be validated in a real deployment. In this thesis, how these models perform in a real life application is analysed. Two models are implemented and

applied in a test-bed located in France.

Table 1.1: The qualitative comparison of the impact of the density regime on various network parameters and performance measures.

	Super-critical (dense) ($\lambda > \lambda_c$)	Phase transition ($\lambda \sim \lambda_c$)	Sub-critical (sparse) ($\lambda < \lambda_c$)
Network capacity	low given no power adaptation	maximum	inside the partitions good, among partitions worst
End-to-end throughput	low	high	low
Connectivity	redundant	edge of chaos: trade-off between throughput and degree	low inside clusters and partitioned network
Allocated bandwidth per node	low	optimal	high but useless
Number of hops	many possibilities to balance trade-offs	minimal	disconnected network
Possibility of multi-path routing	high	very low	none
Delay to sender-to-receiver distance ratio, $\gamma(\lambda)$	scales linearly		scales sub-linearly
Average node degree	high (low deviation)	optimal	low degree (high deviation)
Resilience to link failures	high	low	NA
Redundancy assisted topology control	possible	possible	NA
Trade-off in brief	degraded performance	\longleftrightarrow	disrupted connectivity

1.3 Methodology

In this thesis, two analytical models, namely, RSS based individual density estimator and cooperative density estimator which are proposed by [29] are validated in a real deployment with controlled field experiments. In this study, firstly the problem is explained by considering the importance and necessity of the topic in wireless sensor networks. The problem is specified as a real life implementation for the density estimation issue in large-scale wireless networks inspired by [29]. Then RSS based estimation technique is used for the specified problem. In order to perform the technique in practise, we need a real deployment that consists of hundreds of sensors. We choose IoT-Lab Lille test-bed in city, France to conduct controlled field experiments. Details about the deployment and selected sensor type are presented in Chapter 3. After experiments, the data is obtained to employ the density estimator models. In this thesis, density estimation consists of three steps: path-loss exponent estimation, distance estimation, obtaining results from each estimator. The methods need to find estimated distances to estimate the density [29, 30]. The distance estimation requires path-loss exponent estimation. The results of the estimators are compared with the actual density. In this work, we understood that the calculation of the actual density is also important. We calculate the actual density by using the analytical models. The calculation of the actual density is also explained in this report. By considering the deployment results, a new estimator based on the fusion of the individual and cooperative density estimators is proposed. For the implementations of the estimators MATLAB is used. The detailed experimental results are presented and discussed in Chapter 3.

1.4 Contribution

In this thesis, the density estimators proposed in [29] are validated with controlled field experiments. Moreover, unlike [29], the experiments are made by considering different number of nodes with multiple measurements from their distinct neighbours. Different transmission powers are used, and the experiments are conducted on different parts of the testbed. In addition, since the calculation of actual density is an issue,

unlike [29] we calculate the actual density using well-known distances and employ them to the proposed analytical models, this approach is also more accurate while determining the actual density in a WSN which has a limited-range. At the end, we propose a new estimator that is the fusion of the individual and cooperative density estimators. The new technique is called the fusion density estimation method that yields more accurate results.

1.5 Outline

- In Chapter 2, path-loss exponent estimation and distance estimation techniques in the literature are explained.
- In Chapter 3, density estimation techniques are discussed. Two analytical models proposed as density estimation techniques in [29] are explained in detail. Path-loss exponent estimation which is required by density estimators is also explained.
- In Chapter 4, experimental results are presented and evaluated. We present the chosen test-bed, the topology information about the WSN, types of sensors, collection of the data, distribution of the data, obtained results from analytical models combined with empirical data, and the new fusion approach using both estimators.
- Chapter 5 includes conclusion and future work sections. Conclusion section summarizes the most prominent parts of the work, the evaluation and discussion of the results in a real deployment. Then, the future work section includes suggestions for what to do in the next studies.

CHAPTER 2

RELATED WORK

2.1 Path-Loss Exponent Estimation

In wireless sensor networks, path-loss leads to the variation in received signal strength over distance [15, 31, 37]. The loss of the power emitted by the transmitter as well as by the impacts of the propagation channel [15]. The path-loss exponent is generally assumed identical in a specified distance without considering the effects of the shadowing in the path-loss models [15]. Shadowing, reflection, diffraction, scattering, and absorption are the factors that impact the received signal strength [15, 32, 37, 42].

There are miscellaneous types of path-loss prediction methods in the literature such as free space path-loss model, ray tracing, Okumura model, Hata model, cost Hata 231 model, piecewise linear model, Stanford University Interim (SUI) model, Ericsson model, simplified path-loss model [1, 15, 24, 26, 28, 31, 34, 37, 49]. In this thesis, we choose the simplified path-loss model since we may not know the environment, topology as an outsider statistician. The simplified model needs only the RSS signal strengths and some known distances [10, 15, 22, 29, 33, 45]. The model is particularly explained in Chapter 3. Propagation models are necessary for predicting the path-loss exponent, and they need to be appropriate, low cost and suitable system design alternatives since the site measurements are costly [24, 31]. They can be classified empirical models, site-specific models, theoretical models, indoor and outdoor models [15, 31, 34, 36, 37].

2.1.1 Free Space Path-Loss Model

Assume that no obstructions exist between the receiver and transmitter, and there is a line-of-sight and clear path between them, thus the signal propagation is along a straight line. The free space model estimates that the decays of the received strength as a function of the separation distance of the transmitter-receiver raised to some strength [15, 37]. In this model, the received signal strength lessens in inverse ratio to the square of the distance between receive antennas and transmit antennas. Moreover, the RSS has a ratio of the square signal wavelength, so the power decreases while the carrier frequency increases.

2.1.2 Empirical Path-Loss Models

Some communication systems such as mobile sensor networks that have complex propagation areas cannot be precisely modelled by using the ray tracing or free-space path-loss [1, 24, 26, 28, 31, 34, 37, 49]. Thus, there is a number of empirical models to estimate the path-loss in common wireless topologies such as inside buildings, urban microcells, and urban macrocells. These empirical models basically consist of experimental measurements in a specified frequency range and over a specified distance for a specific environment or building [37]. These empirical models are used for the analysis of the performance in many studies.

2.1.2.1 Okumura Model

This model is the most usual method for signal forecasting in large urban areas [15, 31, 37]. In the Okumura model, the appropriate range of the distance is between 1 and 100 km, but it is possible to extrapolated to 3000 MHz [37] , and the range of the frequency is between 150-1500 MHz. The huge measurements of the base station to mobile signal fading are used by Okumura throughout Tokyo in order to establish a set of curves giving average attenuation with regarded to free space of signal propagation in irregular area. The heights of the base station regarded with these measurements were between 30 m and 100 m. The highest value of this range is higher than the one that belongs to today's common base stations. The upper end of this range is

higher than typical base stations today. The empirical path-loss formula of Okumura [15, 37]:

$$P_L(d)dB = L(f_c, d) + A_\mu(f_c, d) - G(h_t) - G(h_r) - G_{AREA}, \quad (2.1)$$

where d is the distance, and f_c is carrier frequency, $L(f_c, d)$ is free-space path-loss. $A_\mu(f_c, d)$ is the median attenuation besides free-space path-loss across all areas. The height gain factors of the base station antenna and mobile antenna is represented by $G(h_t)$ and $G(h_r)$, respectively. G_{AREA} presents the gain depends on the type of the area. $G(h_t)$ and $G(h_r)$ are found using (2.2 and 2.3 or 2.4):

$$G(H_t) = 20\log_{10}(h_t/200), \quad 30m < h_t < 1000m; \quad (2.2)$$

$$G(H_r) = 10\log_{10}(h_r/3), \quad 10\log_{10}(h_r/3), \quad (2.3)$$

$$G(H_r) = 20\log_{10}(h_r/3), \quad 3m < h_r < 10m. \quad (2.4)$$

2.1.2.2 Hata Model

Hata model in [15, 31, 37] is an experimental formulation based on graphical path-loss data obtained from Okumura and in this model the range of the frequencies is between 150 MHz and 1500 MHz. This model is a closed form formula that simplifies the computation of the path-loss exponent. In the Hata model, the parameters are the same as under the Okumura Model, however the correction factors which are not any path-specific are not provided. This model is appropriate for the earliest-generation cellular systems, and is not suitable for present cellular systems that have higher frequencies and smaller sizes, and indoor environments.

2.1.2.3 COST 231 Extension to Hata Model Model

This model is extended version of the Hata model [15, 31, 37]. The European cooperative for scientific and technical research developed this version to extend the model to 2 GHz. The range of the frequencies of this model is between 1.5 GHz and 2 GHz.

2.1.2.4 Piecewise Linear Model

The Piecewise Linear model in [15] is to design path-loss model in indoor and outdoor areas [15]. This model is a piecewise linear approach based on the dB loss versus log distance. The piecewise linear approximation can be seen in Figure 2.1.

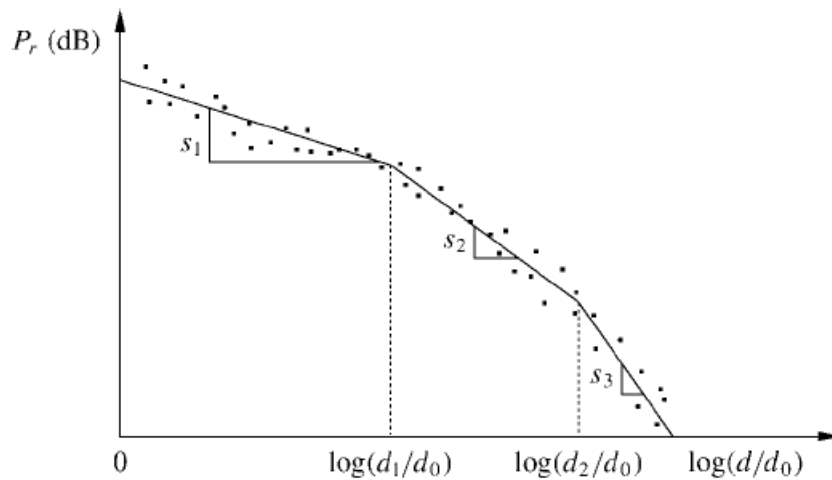


Figure 2.1: Piecewise Linear Model for Path-Loss with dB loss versus log distance.

In Figure 2.1, the dots show the measurements, and the piecewise linear model is used as a methodology to these measurements. Assume that there are M segments in a solution using this model, then the approach must specify $M - 1$ breakpoints d_1, \dots, d_{M-1} besides the slopes corresponding to each segment s_1, \dots, s_M . Different solutions can be applied to determine the location and the number of the breakpoints to be employed in the model. After these are determined, the corresponding slopes for each segment can be calculated by using the linear regression.

2.2 Distance Estimation

There are several methods which are most widely used in recent years such as received signal strength, time of arrival (TOA), time difference of Arrival (TDOA), and hop count [5, 9, 13, 14, 25, 40, 47]. They can be classified as time based distance measurement methods and RSS based methods [14, 40, 47].

2.2.1 Received Signal Strength Based Distance estimation

Received signal strength based distance estimation uses the measurements of the signal strength receiving in a neighbour node and calculates distance employing this received signal strength [5, 9, 13, 14, 15, 25, 29, 37, 40, 47]. In this thesis, the individual and cooperative density estimators uses RSS measurements while calculating the distances by considering the simplified path-loss model. RSS is affected negatively by shadowing, large-scale and small-scale fading [5, 32].

2.2.2 Time of Arrival (TOA)

Assume that a clock synchronization or an exchange timing information by certain protocols exist between two nodes [13, 14, 47]. One node sends a single packet to another node, which contains the time of its transmission. The receiving node knows the time of the arrival of the packet. The distance between these two nodes is calculated by multiplying the velocity of the light and time difference. If this method can be applied, in other words, if the perfect synchronization exists, then it is more accurate than the RSS based method, but due to the the problems of the synchronization, this method is not so popular [13, 14].

2.2.3 Time Difference of Arrival (TDOA)

TDOA is a method that consists of combination of the ultrasound/acoustic and radio signal to predict distances [13, 47]. Like TOA method, this approach also needs the presence of the synchronization. If the synchronization exists between the nodes,

then we can perform this estimation method [13, 14]. The method is based on the hardware ranging mechanism, where each node has a speaker and a microphone [47]. In this method, assume that one source node transmits a radio signal and waits for a fixed interval of time. Then it yields a fixed pattern of "chirps" on its speaker [47]. When the destination nodes receive the signal, they save the current time and turn on their microphones. When their microphones catch the chirp pattern, the destination nodes, they note this current time again. After these measurements are completed then the receivers can calculate the distance between them by employing these measurements together with the speed of the radio and sound waves [47]. In this method, there are some drawbacks due to the possible synchronization problem between the sender time-stamp and the real signal transmission, and the potential delay related to a incoming sound signal being realised at receiver [47].

2.2.4 Hop Count

The hop count method takes the number of hops from source node to the destination node, then multiplies with the maximum communication range of a node [5, 13]. In this method, an unweighed graph is defined by the local connectivity information supported by the radio. In this graph, sensor nodes are the vertices, and direct radio links among nodes are the edges. The hop count between two sensor nodes denotes the length of the shortest path in this graph between these two nodes. In a naive manner, if the hop count, namely, the length between two sensor nodes is less than the result of the multiplication of the maximum communication range and the hop count. The method can give the approximately 20% of the maximum range if the the number of the neighbour nodes are more than 15 [5, 13]. This method provides an accuracy of approximately 50% of the maximum range of a node, then this is a problem for this method [5, 13]. Another problem in this method is that environmental objects may prevent edges from coming in the connectivity graph [5].

2.2.5 Comparison of the distance estimation methods

In Table 2.1, it can be seen that the TDOA has more accurate result, however it is highly required the usage of the hardware [13]. This method may always not be

performed. The RSS technique is the low-cost and the practical approach although it effects negatively large- and small- scale fading, and shadowing. Thus, the RSS based method is a feasible approach [13, 45].

Table 2.1: The Comparison of the Distance Estimation Techniques

		Accuracy		Overhead	
		Line of Sight	Non Line of Sight	Hardware	Computational
Distance Estimation Method	RSS	Low	Very Low	Low	Low
	TOA	High	High	Low	Low
	TDOA	Very High	High	High	Low
	Hop Count	Low	Very Low	Low	Low

CHAPTER 3

DENSITY ESTIMATION

Density estimation in wireless sensor networks is an important issue to take into consideration. Density impacts the performance of the WSN. Many problems in WSNs such as energy conservation through sleep scheduling, topology control for reducing collisions and interference or capacity planning requires precise estimation of density. Density estimation can give beneficial information in some applications such as distribution of mobile devices for crowd management or sensing coverage in a sensor network.

In this chapter, density estimation techniques are discussed. Two proposed analytical models called RSS based individual and cooperative density estimators in [29] are explained in detail. Path-loss exponent estimation that is required by the density estimators is also explained.

3.1 Density Estimation Methods

There are three common approaches for density estimation which are location-based density estimation, neighbour discovery based density estimation and received signal strength based density estimation.

Location-based methods require extra systems such as positioning systems that give the coordinates of wireless tools such as wireless sensors to find the density. For instance, node census [39], density adaptive routing protocol [20], priority-based stateless georouting [46] are methods that find the network density with the location in-

formation of the nodes that is provided by secondary systems such as GPS. There are some disadvantages in this method such that the additional systems need further energy consumption, and the auxiliary systems may lead to errors while estimating the density.

Neighbour discovery based methods make use of the traffic analysis in the network. Traffic analysis [39] or neighbourhood discovery algorithm [21] are some examples. They use the identities of the nodes piggybacked to the packets and collect a census to compute the density. In this method, There are some drawbacks such that the estimation space is limited to the transmission range, and changes on the accuracy of the density estimation depends on the network traffic.

RSS based density estimation methods overcome drawbacks of the previous two methods. In this method, there is no need to use some auxiliary systems, and it is also scalable since the estimation can be calculated locally and the estimation space is controllable [29, 48].

In this thesis, the RSS based density estimation method is chosen. To apply this method, firstly there are three steps, two of them are the path-loss exponent estimation and the distance estimation steps, to be completed. Path-loss exponent estimation lets us to understand the channel propagation model, and it is necessary for the distance estimation. After obtaining the path-loss exponent, the distance estimation step is performed. The final step for each density estimator which is determining of neighbour relations or connectivity degrees. Then, the density estimation methods can be performed by using above results.

3.1.1 Individual Density Estimation

Individual density estimation uses one estimating node and RSS samples from its neighbours while estimating the density. A node measures the RSS of packets transmitted by its neighbours, then (3.1) is used for density estimation. Therefore, the individual density uses only RSS measurements of one node, however, does not use any other collected RSS samples from any other nodes. The individual density esti-

mator is

$$\hat{\lambda} = \frac{n(n+1) - 2}{2\pi \sum_{i=1}^n d_i^2}, \quad (3.1)$$

where $\hat{\lambda}$ is the estimated density, n is the number of the nodes that transmit a packet to the estimating node, and d_i is the estimated distance obtained from (3.2) by using the RSS (dB) values.

In this case, any d_i shows the estimated distance by using:

$$d_i = 10^{\frac{(K+P_t-P_r)}{(10\gamma)}}, \quad (3.2)$$

where K is a constant obtained from (3.3), P_t is the transmission power, P_r is the received power, and γ is the path-loss exponent.

$$K(dB) = 20 \log_{10} \frac{c}{4\pi d_0 f}, \quad (3.3)$$

where f is the frequency and c is the speed of light, and d_0 is the reference distance.

3.2 is a biased estimator. Hence, we use (3.4) for an unbiased estimation. It overcomes the random effects of shadowing [23]:

$$d_i = 10^{\frac{(K+P_t-P_r)}{(10\gamma)}} \left[e^{-\frac{\sigma^2}{2(\frac{10}{\log(10)})^2 \gamma^2}} \right], \quad (3.4)$$

where the σ represents the standard deviation of the log-normally distributed shadowing.

Individual density estimation may not sometimes provide an accurate estimated density. In a sparse network, an estimating node has few neighbours and less measurements, which is reducing the accuracy of the estimator [29].

3.1.2 Cooperative Density Estimation

In a wireless sensor network, each node collects received signal strength measurements from its neighbours. In these measurements, it is possible that there are multiple observations between two nodes. Then, if there exists multiple measurements, the average of them is used for distance estimation by using (2.4). After obtaining the estimated distances (d_j s) among each pair nodes, (3.5) is performed to find the density.

$$\hat{\lambda} = \frac{T}{\pi \sum_{j=1}^n d_j^2}, \quad (3.5)$$

where T represents the summation of the connectivity degrees or the proximity of nearest neighbours, and it can be obtained from (3.6).

$$T = \sum_{j=1}^n k_j, \quad (3.6)$$

where k_j is the connectivity degree of two nodes.

3.2 Path-Loss Exponent Estimation

Density estimators explained above require robust path-loss exponent estimators. Path-loss exponent means difference between the transmitted power and the received power. It shows us the attenuation caused by free space propagation, shadowing, reflection, diffraction and scattering.

In order to estimate the path-loss exponent to analyse the system propagation model, the Simplified Path-loss model in [15] is chosen. This model is used to design easily a single propagation model. Obtaining a model in different environments is not an easy task because of the complex signal propagation. However, we need to estimate the path-loss model without any further information except RSS and some known distances obtained in measurements. This approach provides us a simple way to obtain the path-loss exponent with the measurements. In the literature, there exists already

known path-loss exponents for different environments. These values are shown in Table 3.1 where γ represents the path-loss exponent in Table 3.1.

Table 3.1: Typical Path-Loss Exponents [15]

Environment	γ
Urban macrocells	3.7-6.5
Urban microcells	2.7-3.5
Office building (same floor)	1.6-3.5
Office building (multiple floors)	2-6
Store	1.8-2.2
Factory	1.6-3.3
Home	3

3.2.1 Simplified Path-Loss Model

$$P_r = P_t K \left[\frac{d_0}{d} \right]^\gamma. \quad (3.7)$$

(3.7) can be used for computing path loss as a function of distance where K is a constant, d_0 is the reference distance for the antenna far field, γ is the path loss exponent. P_r is the received power, P_t is the transmission power. d is the transmitter-receiver separation distance [15].

Converting to dB domain, we obtain

$$P_r(dBm) = P_t(dBm) + K(dB) - 10\gamma \log_{10} \left[\frac{d}{d_0} \right], \quad (3.8)$$

where K is a constant and it was obtained by using (3.3), d_0 is the reference distance for the antenna far field, γ is the path loss exponent. The reference distance is chosen as 1 m. When the simplified model is used to approximate empirical measurements, the value of $K < 1$ is sometimes set to the free-space path gain at reference distance [15]. Then, it can be obtained by using (3.3).

While applying the path-loss model, in order to fit to empirical measurements, the MMSE approach is used by performing (3.9) to estimate the path-loss exponent.

$$F(\gamma) = \sum_{i=1}^N [M_{measured}(d_i) - M_{model}(d_i)]^2, \quad (3.9)$$

where N is the number of samples, and the value of γ that minimizes the the mean-square error was calculated by equating the derivative of $F(\gamma)$ to zero, then γ was found.

At this point, again performing (3.9) with the path-loss exponent that is obtained from above steps, we can calculate a sample variance σ^2 as a biased estimate. The result from (3.9) is then divided by the number of samples that is used for calculating the path-loss exponent. σ accounts for the random effect of shadowing.

CHAPTER 4

EXPERIMENTAL RESULTS

In this chapter, experimental results are presented and evaluated. This chapter gives experimental details about which test-bed is chosen, the topology information about the WSN, type of sensors, collection of the data, distribution of the data, obtained results from analytical models processed with empirical data.

4.1 Testbed

In this work, we present the controlled field experiments using IoT-LAB Lille test-bed in France [17].

Lille test-bed is deployed over a 225 m² area, in which there are five offices and a big room separated by a corridor. Nodes are positioned over the ceiling and wood poles. Nodes on ceiling are dispatched over a 1.20 m x 1.20 m grid, at 2.50 m high. Nodes on poles are vertically hanged at 2.40 m, 1.50 m and 0.60 m high.

4.1.1 Deployment

In Lille testbed, two experiments are conducted. The first one is performed on right side of the Lille Testbed. The whole distribution of sensor nodes can be seen in Figure 4.1. The red nodes on ceiling poles are deployed during the first and the second experiments. The deployment of the first experiment is depicted in Figure 4.2. In the second experiment all of the red nodes are used. 30 nodes and 176 nodes are deployed in the first and the second experiment, respectively.

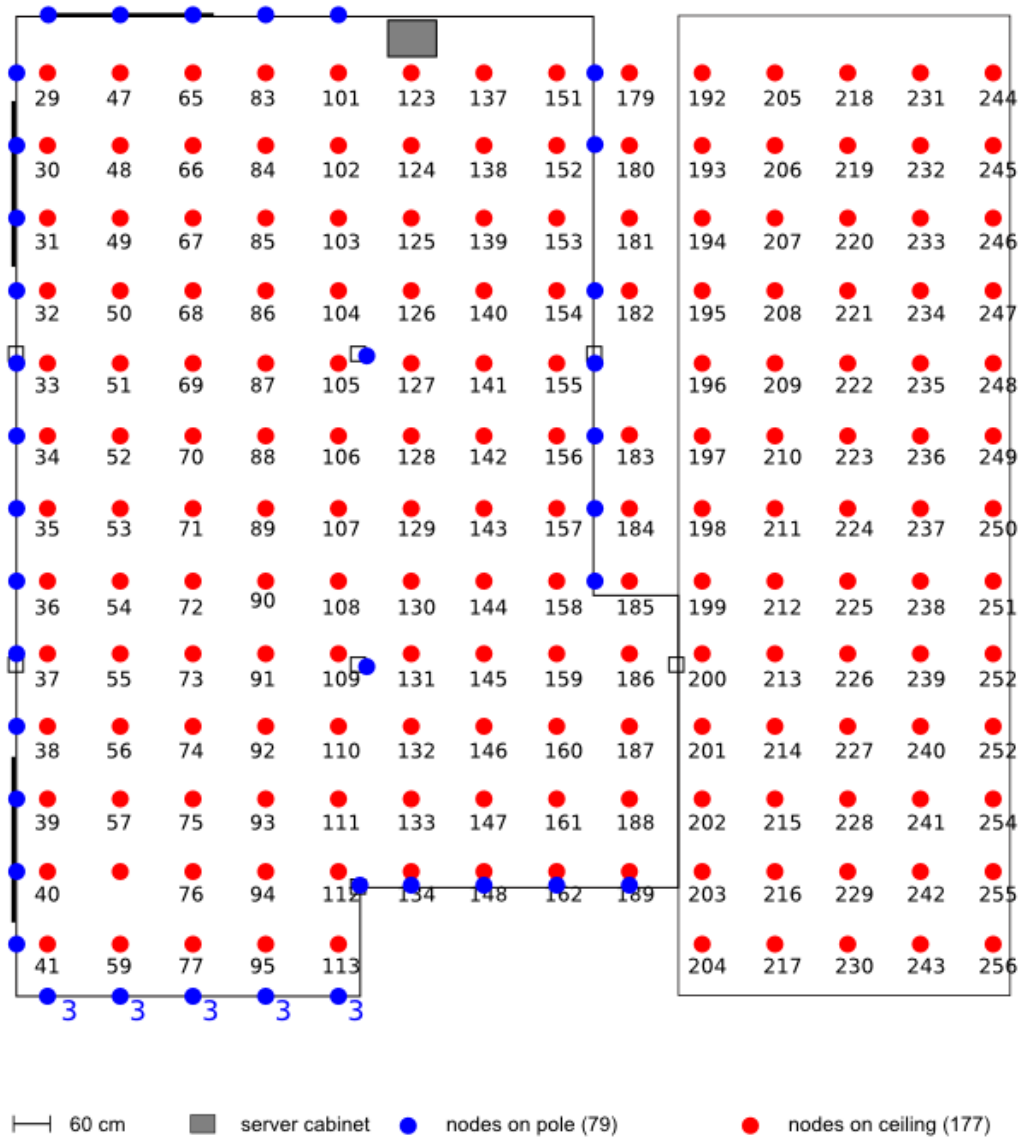


Figure 4.1: Lille Deployment.

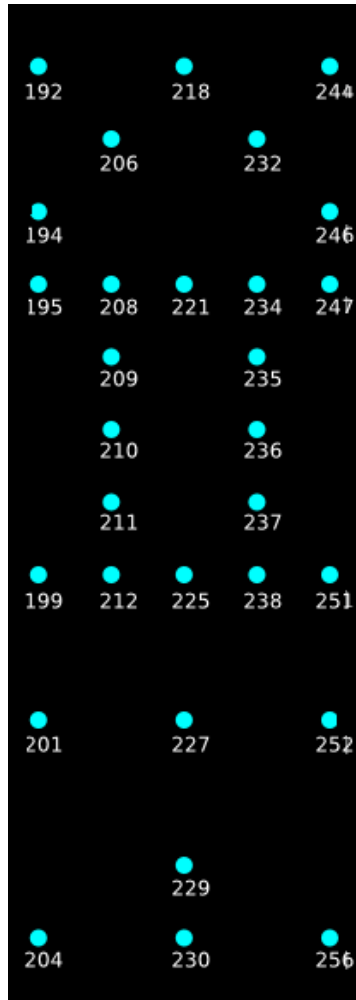


Figure 4.2: Selected Nodes in Lille Deployment in the First Experiment .

4.1.2 Usage of Platform

There are many choices to use the IoT-Lab platform. The web portal and command-line tools are just two of them. Moreover, the platform can be used via a hosted environment on SSH front-ends, CLI Tools which is pre-installed, target architectures cross-compiler tool chains, and accessing to the serial ports of the nodes. The experiment results are accessible in hosted environment. It can be very easy to deploy nodes, and compiling codes and running the experiments; that is why we chose this test-bed.

Figure 4.3 and Figure 4.4 show the web portal user interface and the deployed nodes in the first experiment and the second experiment, respectively.

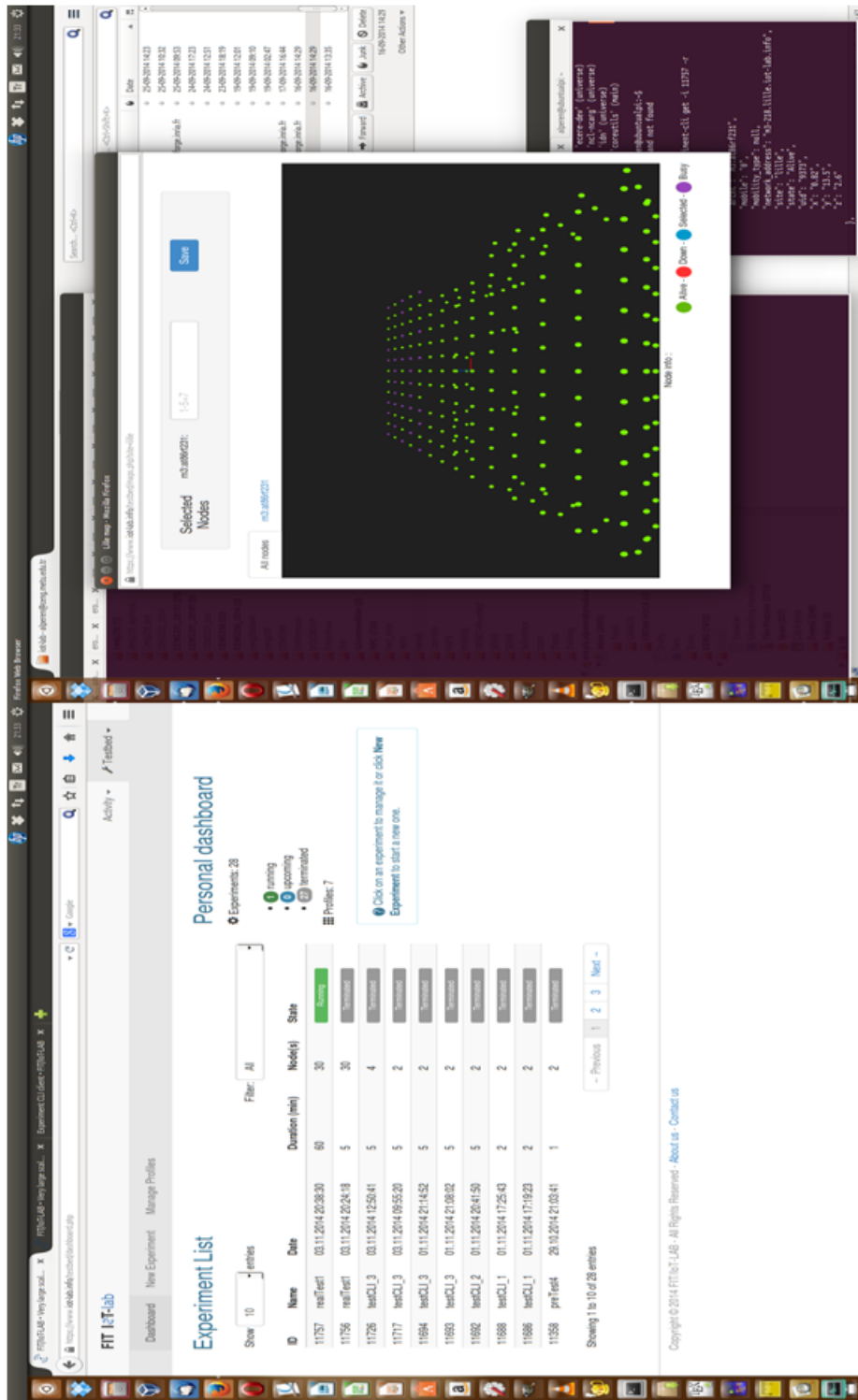


Figure 4.3: A Screen Shot From The First Experiment.

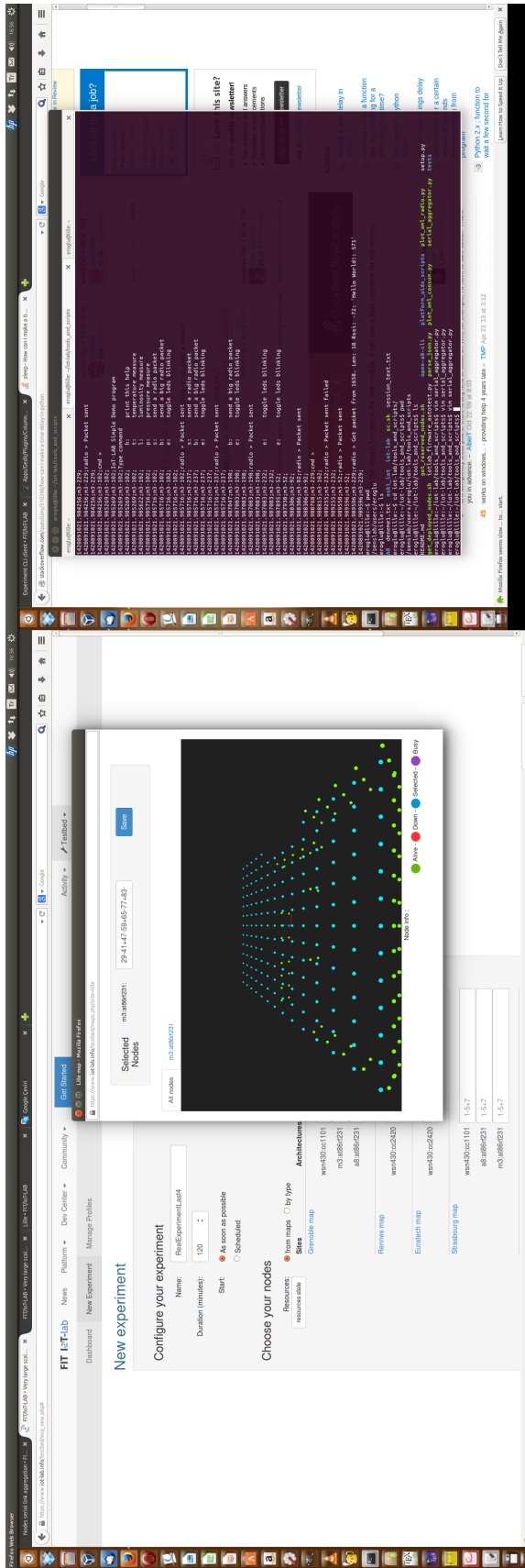


Figure 4.4: A Screen Shot From The Second Experiment.

To understand the system usage, useful tutorials are provided by IoT-Lab web platform. There are a few steps to use this platform: firstly an IoT-Lab account should be created. We can access the web platform of IoT-Lab such as Figure 4.4 after getting the username and password. In the web platform, new experiments can be designed, or some details about old experiments can be seen. Meanwhile, the platform can be used by connecting the IoT-Lab servers. To connect the servers, an RSA key is a requirement. After generating the SSH key, we can register this key by using the "edit my profile" section in the web platform. Then, we can access via typing the code like "ssh username@lille.iot-lab.info" on terminal, in this thesis lille test-bed is used. In the web platform site, after clicking the new experiment button, some configurations should be done such as setting an experiment name, determining the duration of the experiment, and selection of the test-bed and types of the nodes, uploading the binary firmware for the nodes that will be used. Then the submission of the experiment is done.

In the IoT-Lab platform, we can create our own firmware codes by using the SSH front-ends. After connecting the servers, we should select the environment according to types of the nodes. In this thesis, "openlab" environment is chosen since m3 nodes are used. To choose the environment, "make setup-openlab" is typed. In this platform, "gcc-arm" tool chain is used for m3 nodes. Then, the user type "cmake .. -DPLATFORM=iotlab-m3" and "make firmware name" to compile our own code. In this thesis, a implementation based on CSMA MAC library is used. We can access the details of the CSMA MAC code via the following path `/senslab/users/eroglu/iot-lab/parts/openlab/net/mac_csma` in our SSH front-end site. Our firmware consists of some functions such as the "mac_csma_data_send" function for sending a package, the "mac_csma_data_received" function for reception of a package. The transmission power can be changed by setting the "#defineRADIO_POWERPHY_POWER_0dBm". In this thesis two versions of this line are used: "#defineRADIO_POWERPHY_POWER_0dBm" and "#defineRADIO_POWERPHY_POWER_m17dBm". In addition, we can easily get the results of many nodes, and sends beacons to many of them by using "serial link aggregation". In order to obtain the whole nodes results in one terminal, we can use the "serial_aggregator.py" python script. We need to use this script since

we use 30 nodes, 176 nodes in our experiments, otherwise, we have to open a new terminal to get the results for each node. We use this python script within our ssh frontends of the Lille site where the nodes are deployed, and it can be seen in Figure 4.4.

When we want to use the command line tools on our own computer to perform the applications same as SSH front-end in the server. The CLI tools should be installed by following the instructions in tutorials regarded with CLI tools on [17]. Then, we can compile our codes, submit new experiments with managing our profile, selecting the nodes which will be deployed like in the web platform, controlling the status of the running experiment, and looking the list of deployed nodes and accessing their coordinates on this topology. To use the CLI tools, the authentication is also required by using the provided username, password for web platform.

4.2 Data Collection

In this work, two controlled field experiments are conducted. In the first experiment, 30 nodes with default transmission power (0 dBm) are deployed [17]. In the second experiment, 176 nodes with software selectable minimum transmission power (-17 dBm) are used. M3 nodes are used in this test-bed 4.5. The CSMA MAC implementation is used in two experiments. During the experiments, packets are transmitted between each of the deployed nodes.

4.2.1 Data Gathering Devices

The M3 open node is based on a STM32 (ARM Cortex M3) micro-controller [18]. M3 nodes contain a set of sensors and a radio interface such as light, temperature and pressure. Main evolutions are a more powerful 32-bits processing, a new ATMEL radio interface in 2.4 Hz. The node is depicted in Figure 4.5. Moreover, it has ports for Contiki, FreeRTOS and Riot operating systems.

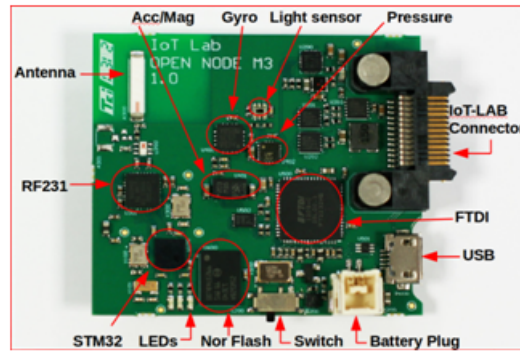


Figure 4.5: m3 Sensor Node[18].

4.2.2 Data Gathering Method

In this work, the data are collected within two experiments. During the experiments, the general-purpose CSMA MAC library which is provided by IoT-Lab platform is used as a low-latency MAC layer. All of the nodes in WSN always have their radio chip in reception mode. If a node is to send a data packet, the node will check whether the radio channel is active or not since another node is transmitting the data, then when the channel is detected as free, the node effectively sends the packet on the air. Using this library a firmware is coded to collect data from each node. We send a packet from each node to the others during the experiments. Empirical data consists of destination node identifiers, source node identifiers, and the RSS value of the packets. In the first experiment, multiple messages are transmitted from each node to the others, which is approximately 100 messages. For the second experiment, 30 messages are transmitted among the 176 nodes.

4.2.3 Data Manipulation

Firstly, for each experiment the empirical data are divided into two parts: the first part of the data called train data is used for path-loss exponent estimation, and the second part of the data called test data is used while performing the individual and cooperative density estimation techniques. The train data are composed of approximately 1/3 of the whole experiment data. The rest of the data is used for calculating the results of the estimators. The collected and modified data includes destination node identifiers, source node identifiers, RSS value of the packets, and the distance between destina-

tion and source node. The actual distances are calculated by using the coordinates of the nodes. In this topology, each node has a unique identifier, and nodes on ceiling are dispatched over a 1.20 m x 1.20 m grid, at 2.50 m high. Therefore, we can know which node send messages to the other node, and what the distance is between these two nodes. The train data is composed of 31620 samples in the first experiment and 332722 samples for the second experiment. The test data consists of 66981 observations, and 663845 observations in the second experiment. The sample distribution of the train and test data are depicted in Figure 4.6, 4.7 and 4.8. Before using the data, we also apply outlier detection for each part of the data. We define an outlier as a value that is more than one standard deviation away from the mean.

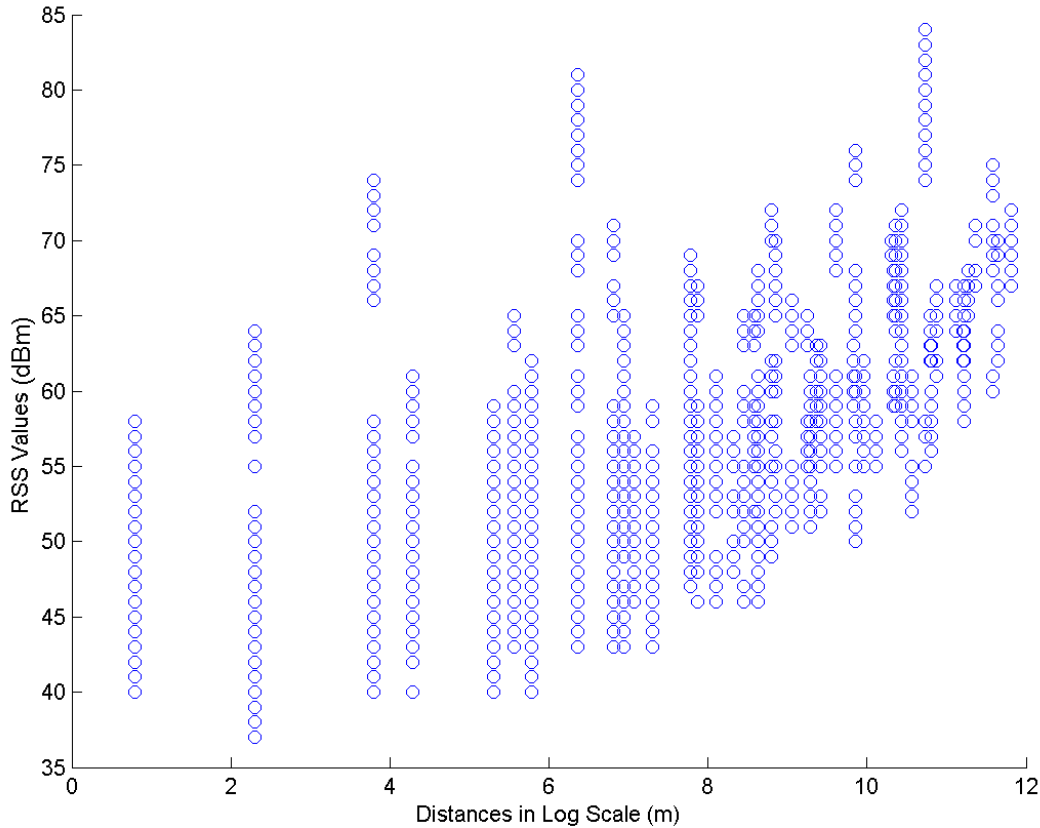


Figure 4.6: Train Data in Logarithmic Scale with 0 dBm Transmission Power.

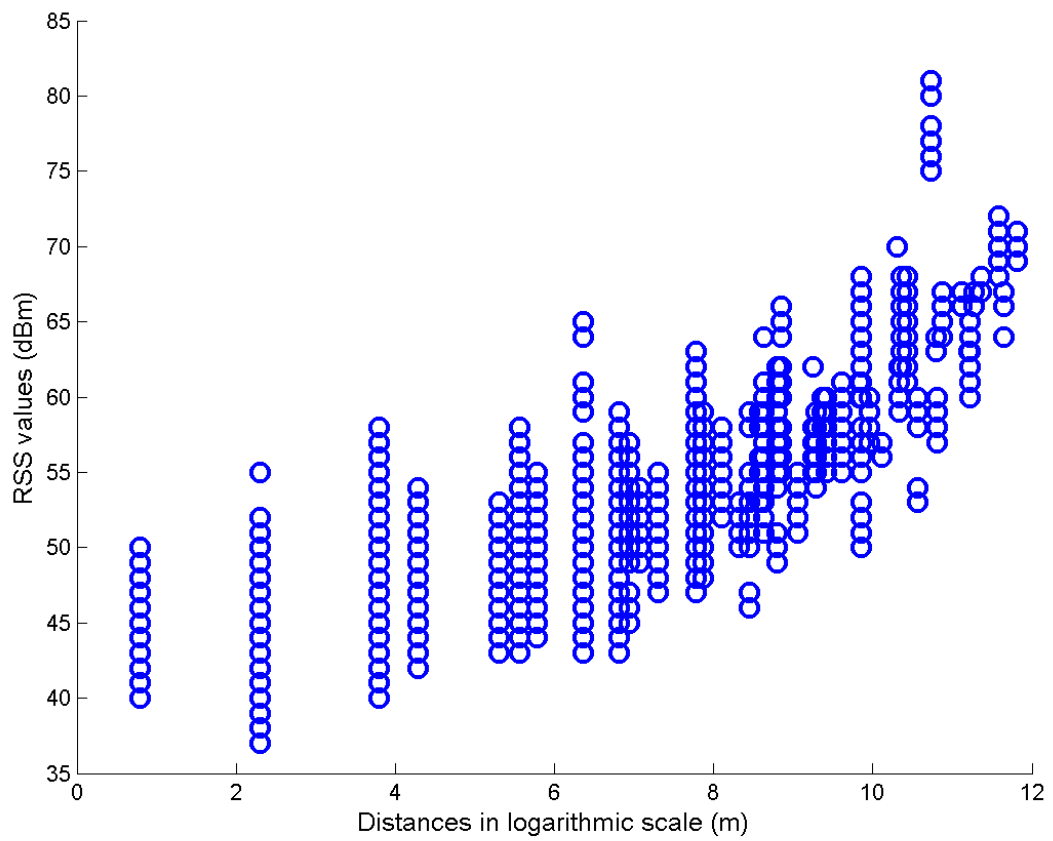


Figure 4.7: Test Data in Logarithmic Scale with 0 dBm Transmission Power.

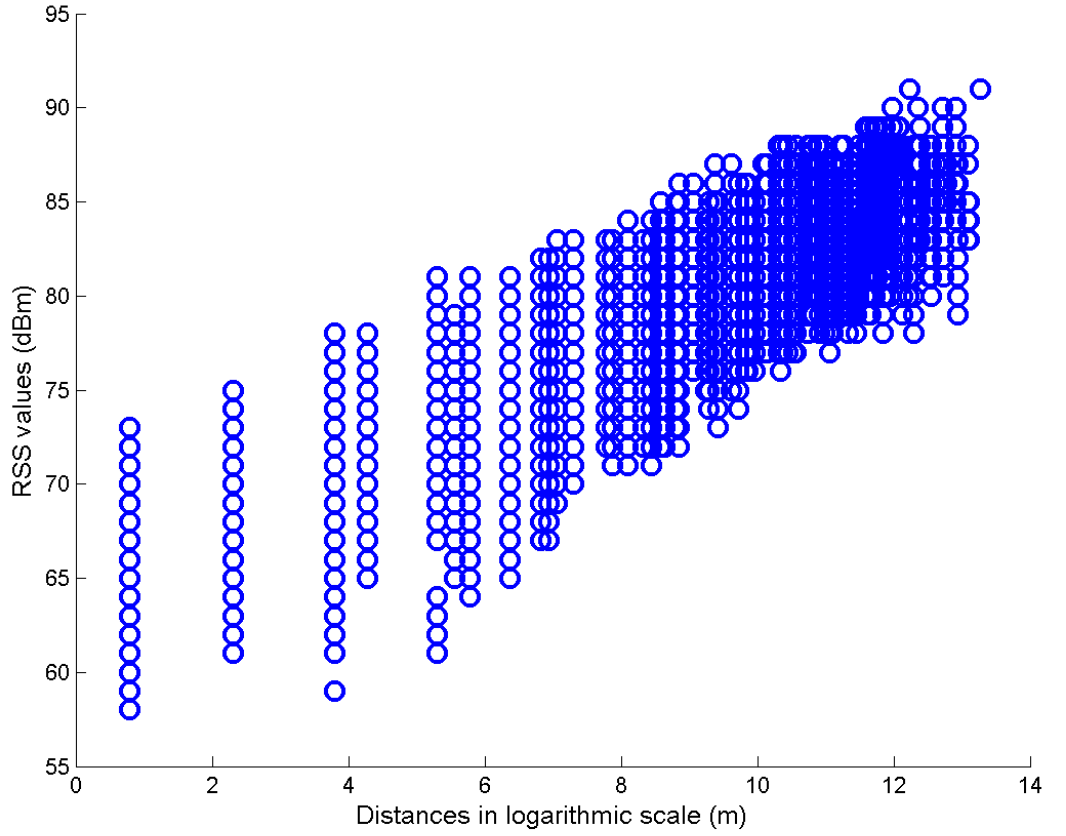


Figure 4.8: Test Data in Logarithmic Scale with -17 dBm Transmission Power.

Secondly, dBm to mW conversions is performed on the train data. After converting RSS (dBm) values to mW by using (4.1), the unique distances between nodes are found. Then for each unique distances, the average of RSS values is found since there exists multiple measurements for a node. At the end of this step, there are max 48 unique distances and RSS values for the first experiment, and max 92 unique distances and RSS values for the first experiment. After that RSS (mW) values are converted to (dB) values by using (4.2).

$$P_{(mW)} = 10^{(P_{dBm}/10)}. \quad (4.1)$$

$$P_{(dB)} = 10 \log_{10} \left(\frac{P_{(mW)}}{1_{(mW)}} \right). \quad (4.2)$$

The obtained data after these steps is depicted in Table 4.1 and Table 4.2

There exists 48 and 92 unique euclidean distances among the nodes for each experiment when train data in each experiment is used to estimate the path-loss exponent.

Table 4.1: Unique Distance Values and Their Average RSSs for the First Experiment.

Distance(m)	RSS(dB)	Distance(m)	RSS(dB)
1.20	-43.92	8.65	-59.08
1.70	-43.26	8.74	-56.34
2.40	-45.70	9.14	-57.73
2.68	-46.10	9.60	-60.25
3.39	-46.34	9.67	-55.89
3.60	-48.21	9.90	-58.05
3.79	-47.83	10.25	-56.42
4.33	-49.51	10.73	-69.80
4.80	-50.10	10.80	-61.19
4.95	-48.55	10.87	-64.04
5.09	-50.87	11.06	-62.74
5.37	-49.35	11.38	-55.37
6.00	-52.62	11.82	-60.81
6.12	-53.00	12.00	-63.29
6.46	-52.81	12.06	-58.77
6.79	-51.57	12.24	-64.30
7.00	-51.25	12.92	-66.06
7.20	-55.94	13.20	-63.09
7.30	-54.44	13.25	-61.80
7.59	-54.78	13.42	-66.01
7.68	-57.55	13.68	-67.71
8.05	-54.32	14.40	-64.91
8.40	-56.82	14.60	-65.36
8.49	-55.58	15.18	-69.68

Table 4.2: Unique Distance Values and Their Average RSSs for The Second Experiment

Distance(m)	RSS(dB)	Distance(m)	RSS(dB)	Distance(m)	RSS(dB)
1.20	-65.31	10.18	-80.94	14.84	-85.33
1.70	-68.10	10.25	-80.51	15.04	-82.57
2.40	-69.56	10.32	-80.37	15.18	-84.82
2.68	-70.51	10.73	-80.56	15.27	-82.16
3.39	-71.30	10.80	-80.23	15.37	-83.20
3.60	-71.38	10.87	-81.23	15.60	-85.16
3.79	-72.94	11.06	-81.18	15.65	-84.12
4.33	-73.84	11.32	-82.00	15.78	-88.52
4.80	-73.86	11.38	-81.36	16.01	-86.50
4.95	-74.44	11.82	-82.08	16.10	-85.21
5.09	-74.95	11.88	-81.42	16.14	-83.37
5.37	-74.90	12.00	-81.77	16.32	-83.53
6.00	-76.55	12.06	-81.99	16.67	-82.93
6.12	-76.36	12.24	-81.84	16.71	-87.97
6.46	-77.30	12.35	-82.33	16.97	-82.61
6.79	-77.71	12.53	-81.92	17.06	-83.35
7.00	-77.50	12.76	-81.27	17.18	-87.12
7.20	-77.40	12.92	-82.23	17.31	-85.43
7.30	-77.32	12.98	-82.72	17.72	-85.54
7.59	-77.75	13.20	-83.26	17.84	-84.23
7.68	-78.25	13.25	-82.51	18.00	-84.95
8.05	-79.44	13.42	-82.20	18.32	-85.52
8.40	-78.30	13.58	-82.85	18.67	-86.64
8.49	-78.39	13.68	-82.62	18.74	-85.75
8.65	-78.92	13.99	-82.05	18.97	-86.44
8.74	-79.43	14.05	-83.39	19.53	-87.25
9.14	-80.14	14.40	-83.92	19.68	-85.65
9.37	-79.62	14.45	-82.79	20.36	-86.54
9.60	-79.23	14.50	-83.96	20.44	-84.28
9.67	-80.30	14.60	-84.97	21.23	-91.00
9.90	-80.69	14.65	-82.24		

The relation between the unique distances and their corresponding average of RSS values in logarithmic scale is shown in Figure 4.9.

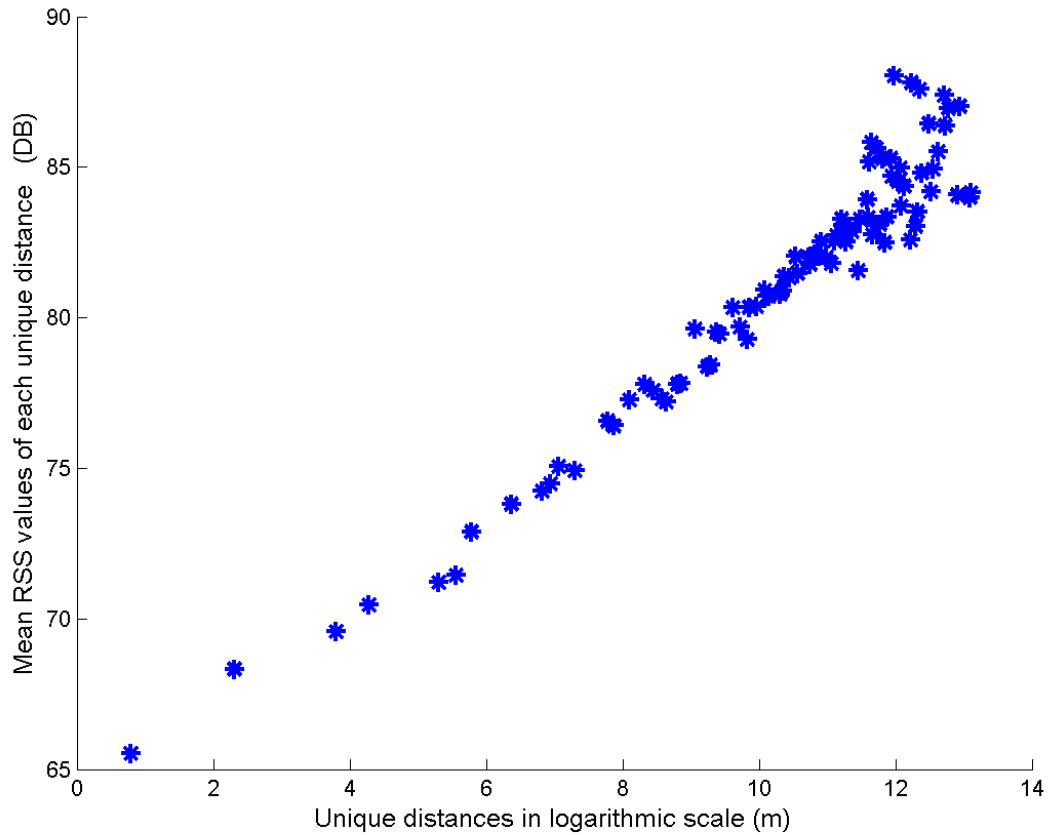


Figure 4.9: Unique Distances in Logarithmic Scale vs Their Average RSS values in -17dBm Transmission Power.

After obtaining the results in Table 4.1 and Table 4.2, the simplified path-loss model that is presented with (3.8) is performed. The reference distance is chosen 1 m. Then, the K value in (3.2) is computed by using (3.3), and K is found as -40.046 dB. While applying the path-loss model, in order to fit to empirical measurements, the MMSE approach is used by performing (3.9) to estimate the path-loss exponent.

At this point, the sample variance can be calculated [37]. Table 4.3 shows γ and sample variance (σ) values while different number of nodes are used.

Table 4.3: Path-Loss Exponent Estimation Results with Different Number of Nodes with 17 dBm Transmission Power.

Number of Nodes	Sigma(σ)(dB)	Path-Loss(γ)
5	5.71	2.52
15	4.57	2.37
25	3.48	2.36
35	3.20	2.28
45	2.45	2.35
55	2.81	2.36
65	2.33	2.31
75	2.24	2.32
85	2.21	2.27
95	1.89	2.33

4.2.4 Evaluation of Path-Loss Exponent

A robust path-loss exponent is important while using RSS based density estimation methods. After estimating the path-loss exponent model, we can have an information about the signal propagation in WSN that is used for controlled field experiments. In this experiment, we know the distances between each node. How can we estimate γ when the deployment is not known. Let assume we want to calculate the number of access points in a building. Firstly, we have to collect the RSS samples from some access points by specifying the distances. After determining the distances, we can collect the RSS values, but it is important that we have to use a constant transmission power during the data collection. Then, by using the RSS samples with well known distances, a regression analysis can be done to estimate the path-loss exponent. For some known distances and their RSS values, we find the slope that is the the path-loss exponent.

The accuracy of the path-loss exponent needs to be evaluated since it is important to see how the signal propagation model is in that environment. Our path-loss exponent should have the same range as the path-loss values of a same floor in Table 3.1. In can be seen that the obtained path-loss exponents while different number of nodes in Table 4.3. Moreover, after path-loss exponent estimation completes, we can estimate

distances with the RSS values in dB scale. By using some well-known distances we can see whether the estimated distances and real distances converge or not in Figure 4.10. It can be seen that the path-loss exponent estimation is mostly accurate.

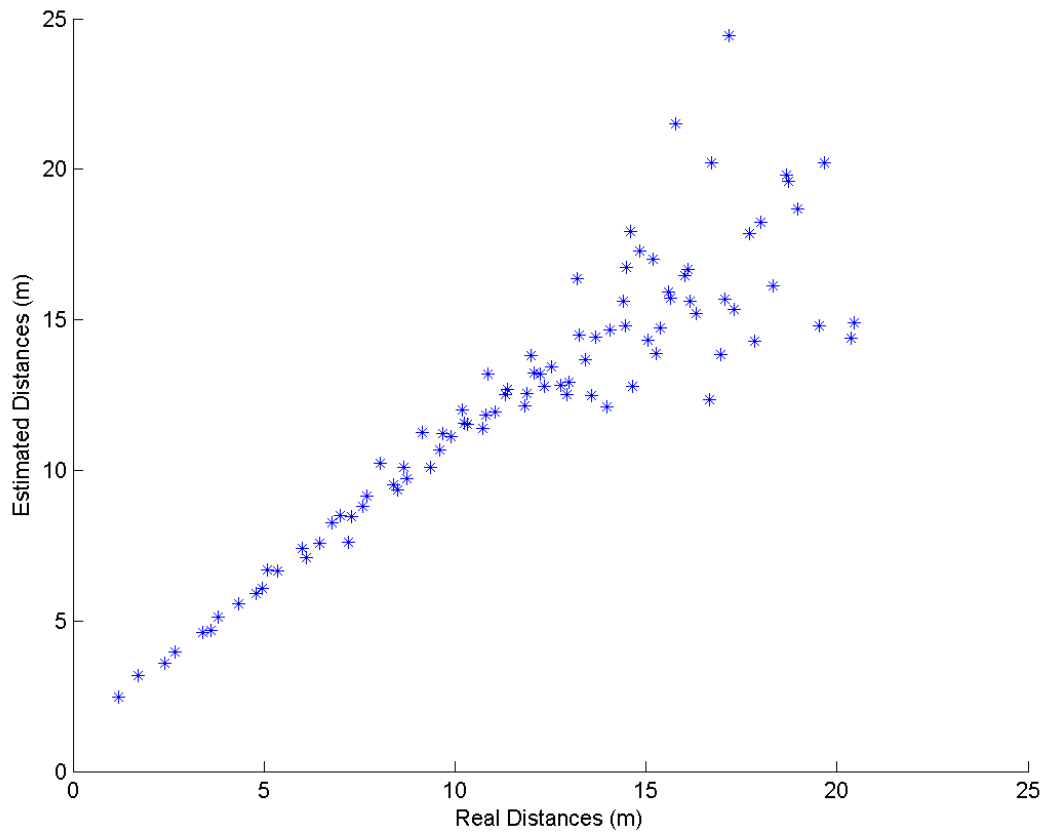


Figure 4.10: Real Distances vs The Average of Estimated Distances with -17dBm Transmission Power.

4.3 Results of Cooperative Density Estimation

Cooperative density estimation results are obtained by using the measurements of each node. We increase the number of nodes each time for the graphical results of the experiments. Cooperative density estimation results are analysed for two empirical data, namely when the transmission power is 0 dBm, and when the transmission power is -17 dBm. The number of nodes obtained from the first empirical data is ranging from 5 nodes to 30 nodes, and the other results are obtained by increasing

the number of nodes from 20 to 160 nodes. When the selected transmission power is -17 dBm, the communication range is smaller; on the contrary, when the transmission power is 0 dBm, the communication range is large. Large communication ranges may cause an increase by alleviating the border effect problem, consequently the accuracy of the estimators is low in the first experiment when the transmission power is 0 dBm.

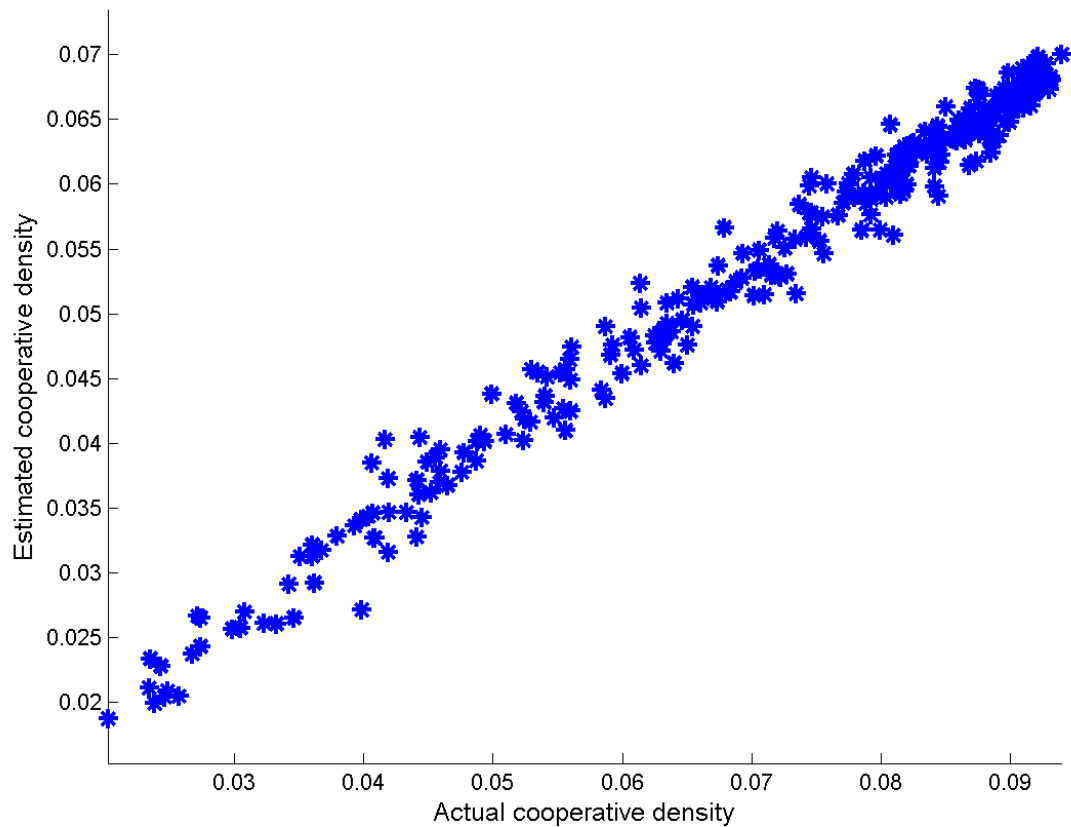


Figure 4.11: Actual Cooperative Density vs. Estimated Cooperative Density Scatter Plot I when Transmission Power is -17 dBm.

The relation between the actual cooperative density estimation and the estimated cooperative density is shown in Figure 4.11. When the network is sparse, there is a slight underestimation of the density. However, as the network becomes denser, the level of the underestimation increases. Each node in this deployment has a noise because of the multi-path fading and border effect problem. When the number of nodes increases, the amount of noise also increases. This problem can be managed by overcoming these phenomena.

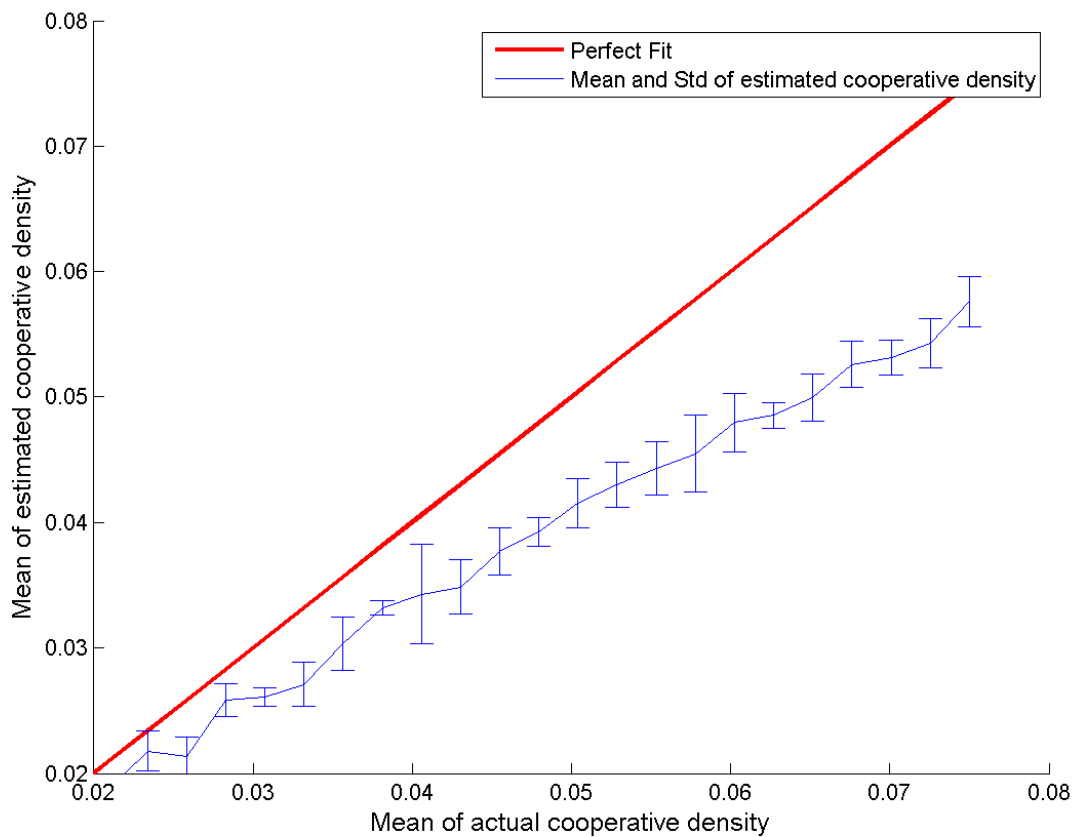


Figure 4.12: Actual Cooperative Density vs. Estimated Cooperative Density Error Bar I when Transmission Power is -17 dBm.

The results are shown with the 95% confidence intervals in Figure 4.12. The level of the confidence interval can be seen in this figure. It can be seen that the result of cooperative density estimation stay under the perfect fit; that is, it underestimates the density. In sparse deployments, namely when the number of nodes is small, the results of the cooperative density estimators and actual density are closer. However, as the actual density increases, the accuracy of the estimator is affected negatively. The accuracy of the estimator is getting lower while the network density increases, since the cooperative density estimators use all selected nodes and their RSSs. Because of the shadowing, multi-path fading, and RSSs with noise, the estimator is performing poorly. Furthermore, since we collect RSS measurement from overlapping areas, the measurements are highly correlated. The correlation of the data negatively impacts the accuracy of the estimators.

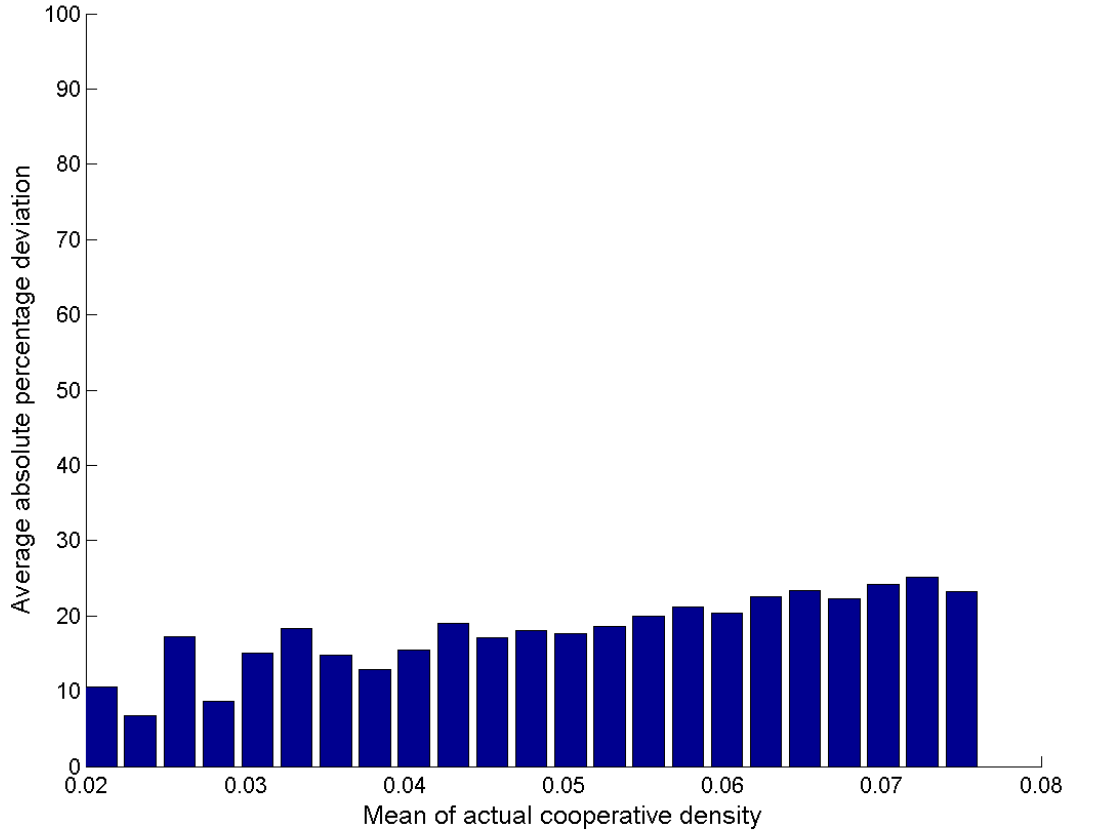


Figure 4.13: Cooperative Density vs. Average Absolute Percentage Deviation I when Transmission Power is -17 dBm.

We present the average absolute percentage deviation (AAPD) from actual density in Figure 4.13. The AAPD is a measure of accuracy, and the AAPD represents the accuracy as a percentage. It can be seen that the average of the AAPD of the estimate is about 20%. The AAPD is defined as

$$AAPD = \frac{100}{n} \sum_{t=1}^n \left(\frac{|\lambda - \hat{\lambda}|}{\lambda} \right), \quad (4.3)$$

where n is the number of samples, λ is the actual density, $\hat{\lambda}$ represents the estimated density.

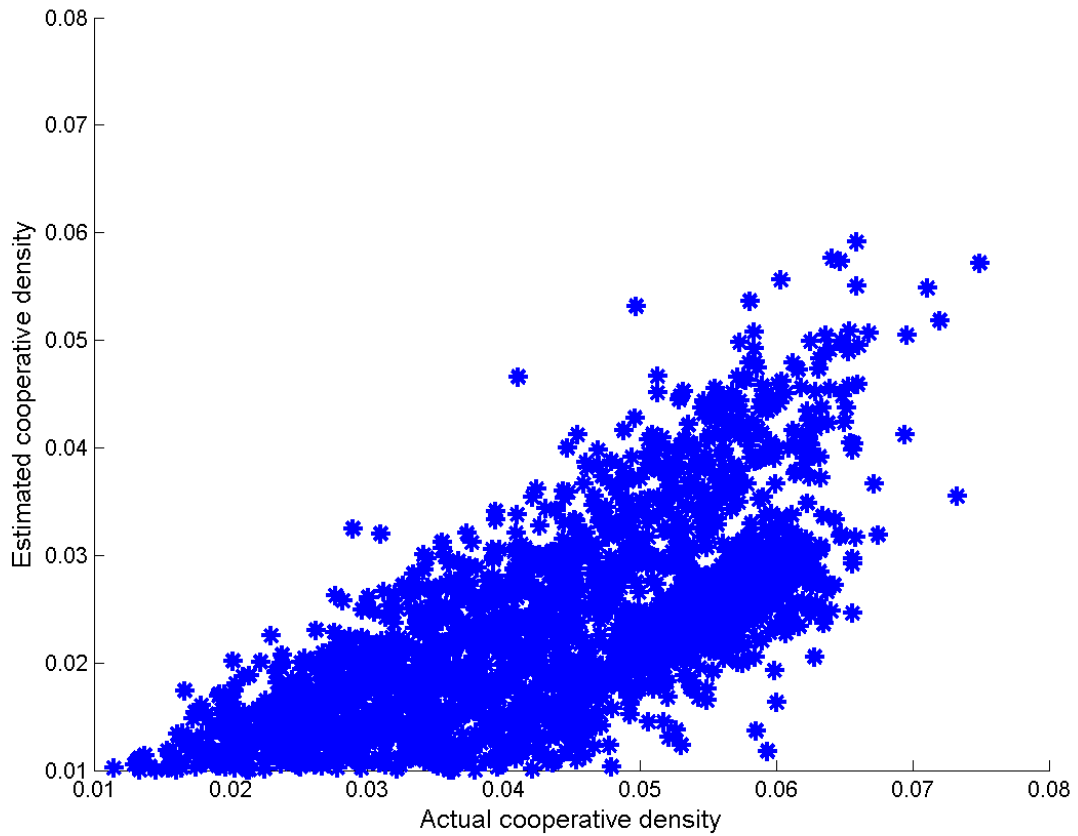


Figure 4.14: Actual Cooperative Density vs. Estimated Cooperative Density Scatter Plot II when Transmission Power is 0 dBm.

Actual density versus the estimated cooperative density when the transmission power is 0 dBm is shown in Figure 4.14. As it was the case when the transmission power was -17 dBm, we under estimate the density when a larger amount of transmission power is employed. However, as the transmission power increases, the AAPD increases considerably as we will present in the sequel.

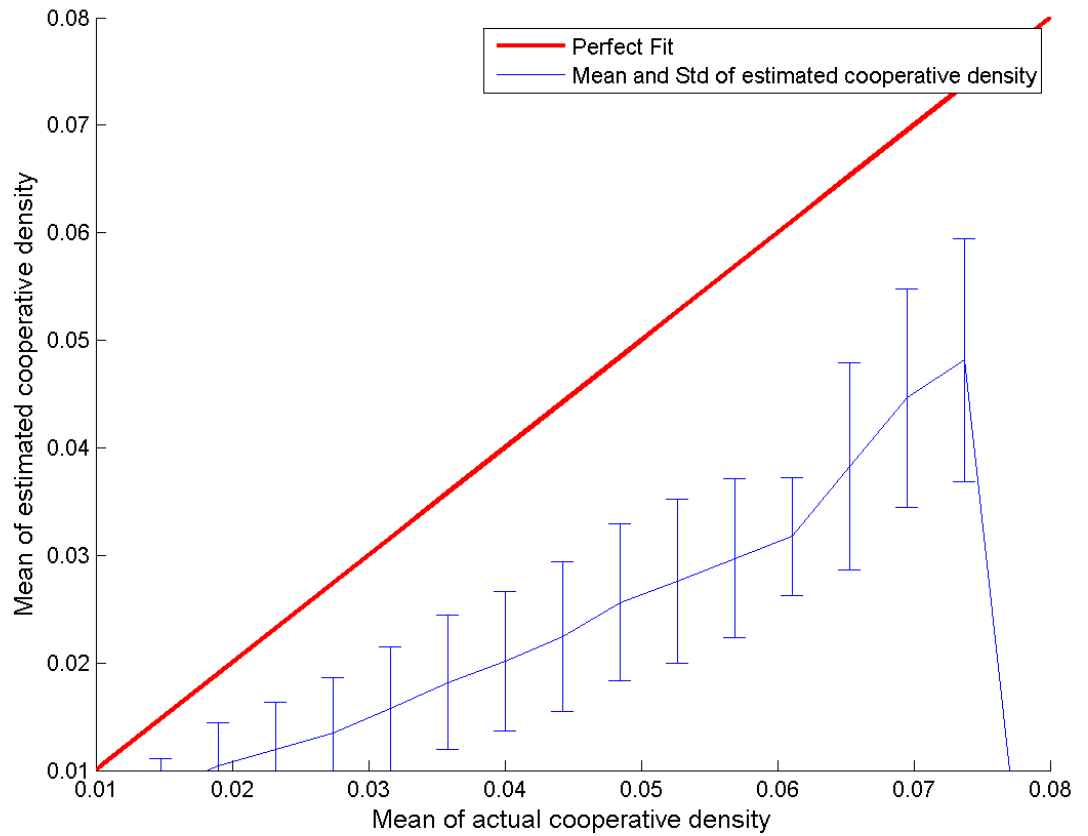


Figure 4.15: Actual Cooperative Density versus Estimated Cooperative Density Error Bar II when Transmission Power is 0 dBm.

The results are presented with the 95% confidence interval in Figure 4.15 when the transmission power is 0 dBm. In this experiment, the maximum number of nodes is 30. At each run, the density estimator randomly selects 5 nodes in initial step, and 30 nodes at the end. Since we select different nodes at each run, the actual density and the estimated density values change. To present the results, we divide the density range into bins and accumulate the results for each bin. The estimated densities for each bin is averaged and presented in Figure 4.15. The maximum number of nodes in the topology is 30. Therefore, when we select all the 30 nodes in the runs, we obtain the same actual density and the same estimate. That is why, there happens to be sudden jumps in Figure 4.15.

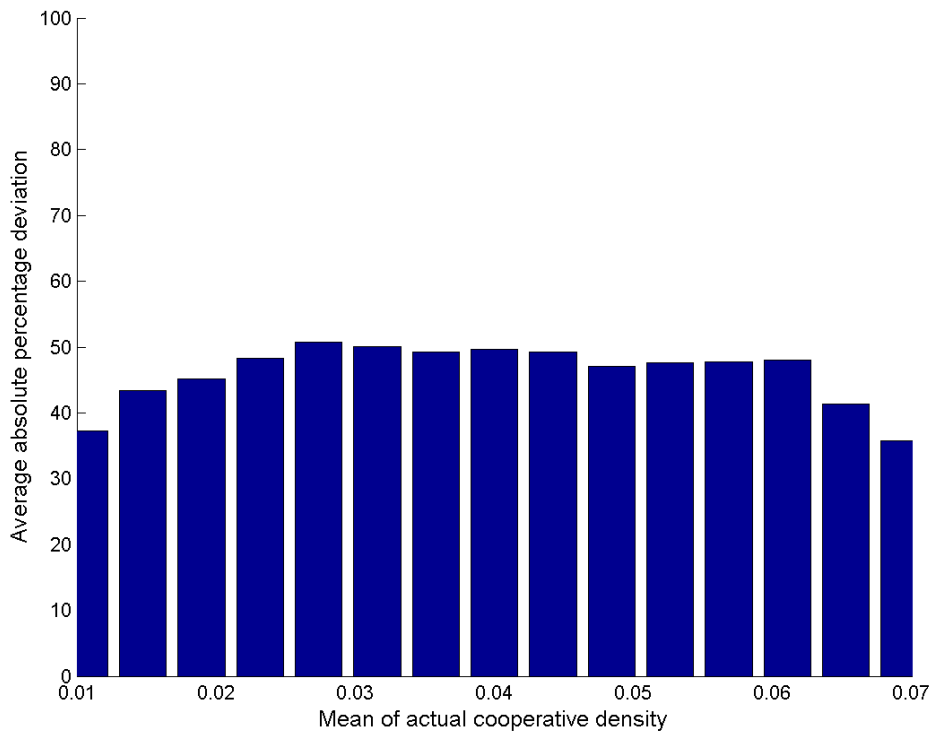


Figure 4.16: Cooperative Density vs. Average Absolute Percentage Deviation II when Transmission Power is 0 dBm.

The results are represented in terms of average absolute percentage deviation (AAPD) from actual density in Figure 4.16 when the transmission power is 0 dBm. The results of the AAPD show that the accuracy of the cooperative density estimator is lower as it was the case in the previous experiments when the transmission power was -17 dBm. In this experiment, there exists 30 nodes in Figure 4.2, and RSS values of deployed nodes have a lot of noise because of the border-effect problem and multi-fading, and default transmission power 0 dBm. The average of the AAPD is about 40%. As the transmission power increases, the communication ranges of the nodes increases and the empty regions around the deployment area significantly impacts the accuracy of the estimator.

4.4 Results of Individual Density Estimation

Individual density estimation uses only measurements of one node that is selected in the middle of the deployment area as the estimator node. Individual density estimation results are also analysed for two empirical data, namely when the transmission power is 0 dBm, and when the transmission power is -17 dBm. The range of the number of nodes obtained from the first empirical data is increased from 5 nodes to 30 nodes, and the other results are obtained by increasing the number of nodes from 20 nodes to 160 nodes. When the selected transmission power is -17 dBm the, the communication range is smaller, on the contrary in 0 dBm, the communication range is large, this may cause an increase in terms of the border effect problem, so the accuracy of the estimators is more lower in the first experiment with 0 dBm. For the individual density estimation, the node labelled 143 in Figure 4.1 for the second experiment in -17 dBm, and the node labelled 232 in Figure 4.2 for the first experiment are selected as estimating nodes.

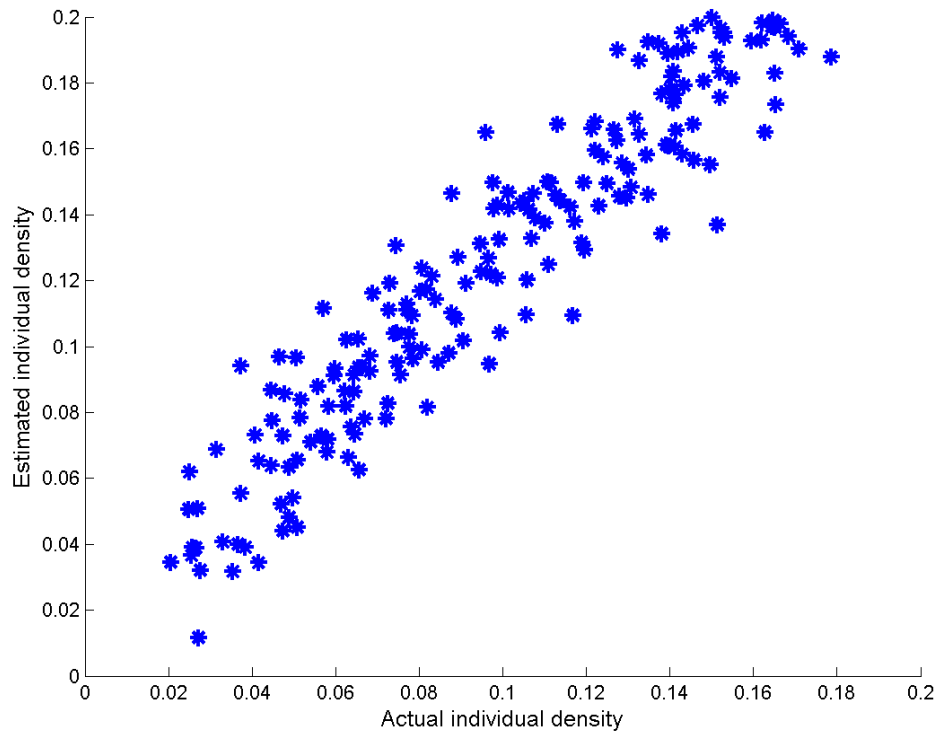


Figure 4.17: Actual Individual Density vs. Estimated Individual Density Scatter Plot I when Transmission Power is -17 dBm.

The relation between the actual individual density estimation and estimated individual density estimation can be seen in Figure 4.17. It can be seen that there is an overestimation. The degree of the overestimation is increasing while the network is getting dense. In individual estimation, the estimator node collect the RSS measurements only from its direct neighbours. Consequently, the measurements are highly correlated with each other. In cooperative estimation, the errors introduced by some nodes could be suppressed by the measurements from other nodes. However, in individual estimation, this implicit error suppression is not possible since we use the measurements collected only by the estimating node.

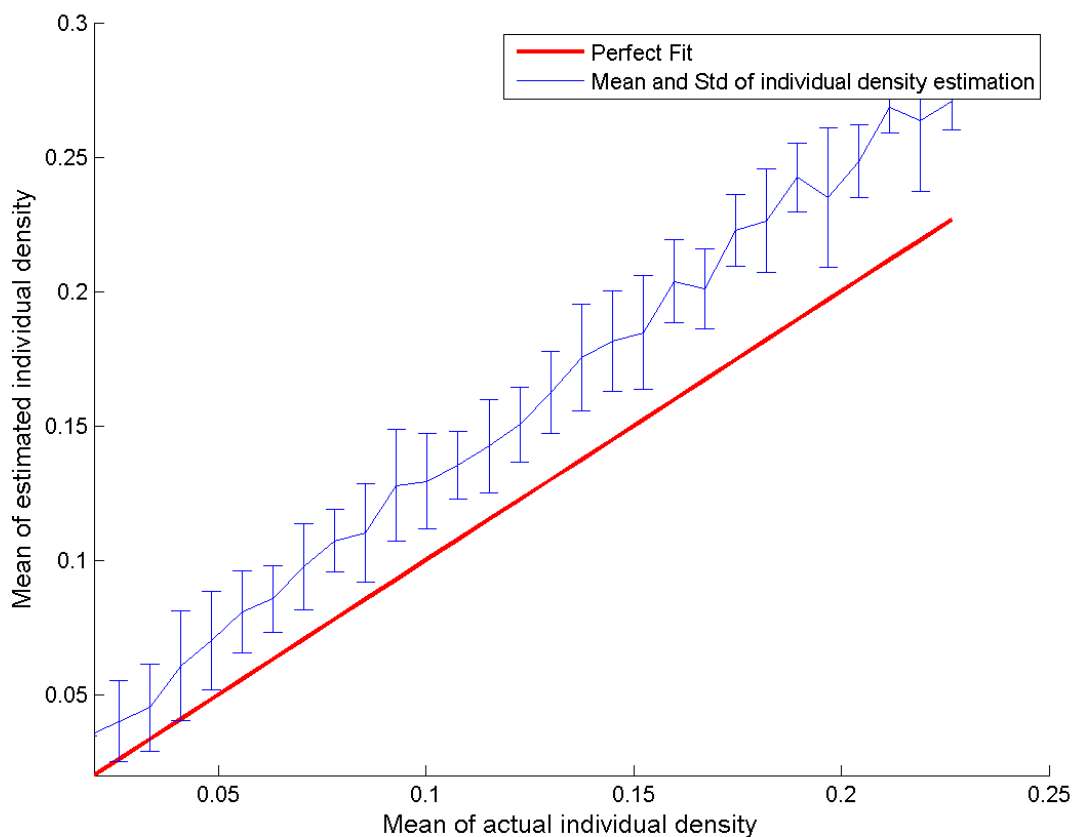


Figure 4.18: Actual Individual Density vs. Estimated Individual Density Error Bar I when Transmission Power is -17 dBm.

The results are represented by using the 95% confidence interval in Figure 4.18 when the transmission power is -17 dBm. It can be seen that the result of individual density estimation stay over the perfect fit (overestimation). We observe a positive bias in the

density estimates due to correlated RSS measurements as explained above.

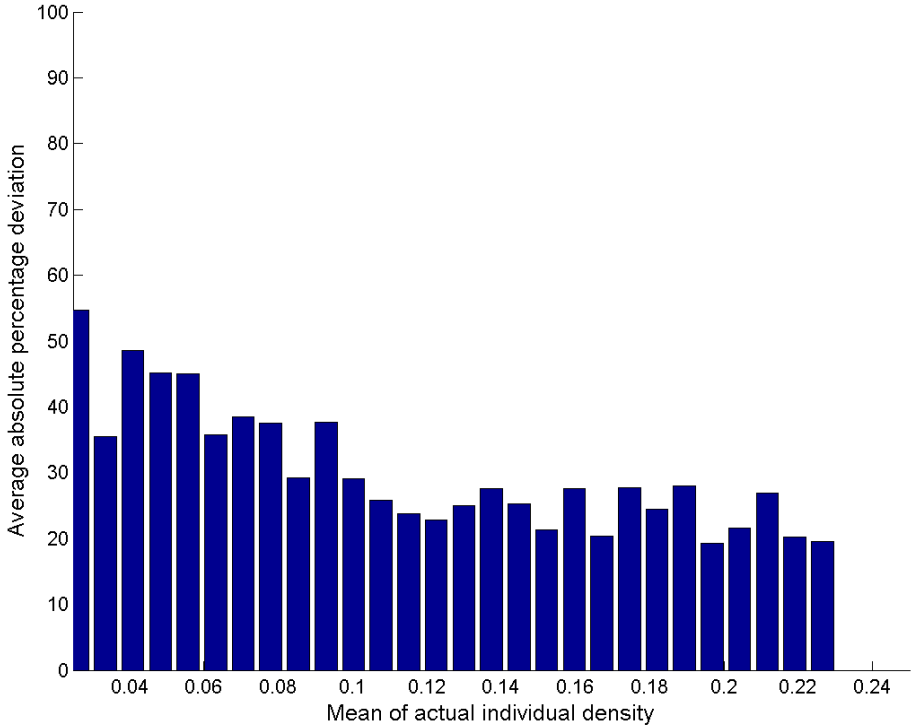


Figure 4.19: Individual Density vs. Average Absolute Percentage Deviation I when Transmission Power is -17 dBm.

The results are shown in terms of average absolute percentage deviation (AAPD) from actual density in Figure 4.19. The results of the AAPD show that the accuracy of the cooperative density estimator is low that the previous result in the experiment when the transmission power is -17 dBm. The average of the AAPD is about 20%.

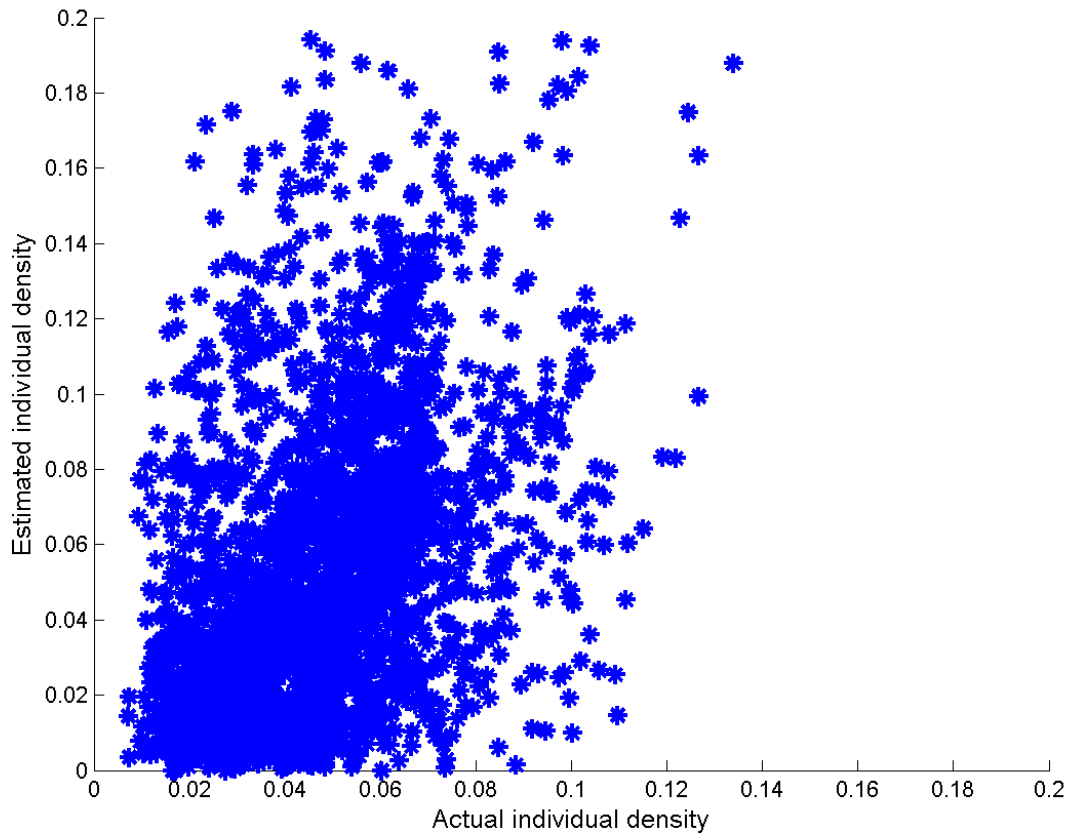


Figure 4.20: Actual Individual Density vs. Estimated Individual Density Scatter Plot II when Transmission Power is 0 dBm.

Figure 4.20 shows the scatter plot of the actual individual density versus estimated individual density. In this experiment, the transmission power is 0 dBm and the range of the deployed nodes is between 5 and 30, in addition the node labelled 232 in Figure 4.2 is selected. In this case the individual density estimator under-estimates at initial steps, however in the next steps when the number of nodes became grater than 15 nodes, the estimator over-estimates.

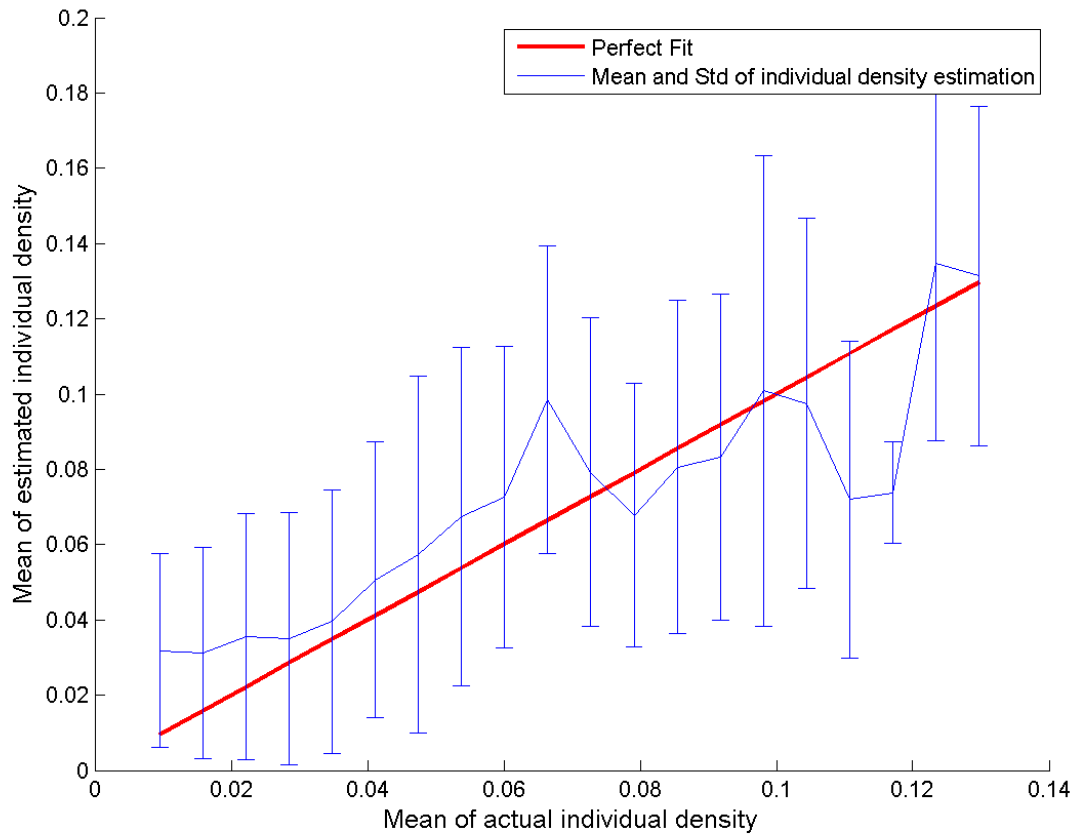


Figure 4.21: Actual Individual Density vs. Estimated Individual Density with 95 confidence interval when Transmission Power is 0 dBm.

The results are shown by using the 95% confidence interval in Figure 4.21. When the number of nodes in Figure 3.2 is greater than 15 nodes the individual density estimator converges the perfect fit, then under-estimates. If the number of selected nodes whose RSSs are less noisy increases, the estimation is getting more closer to fit.

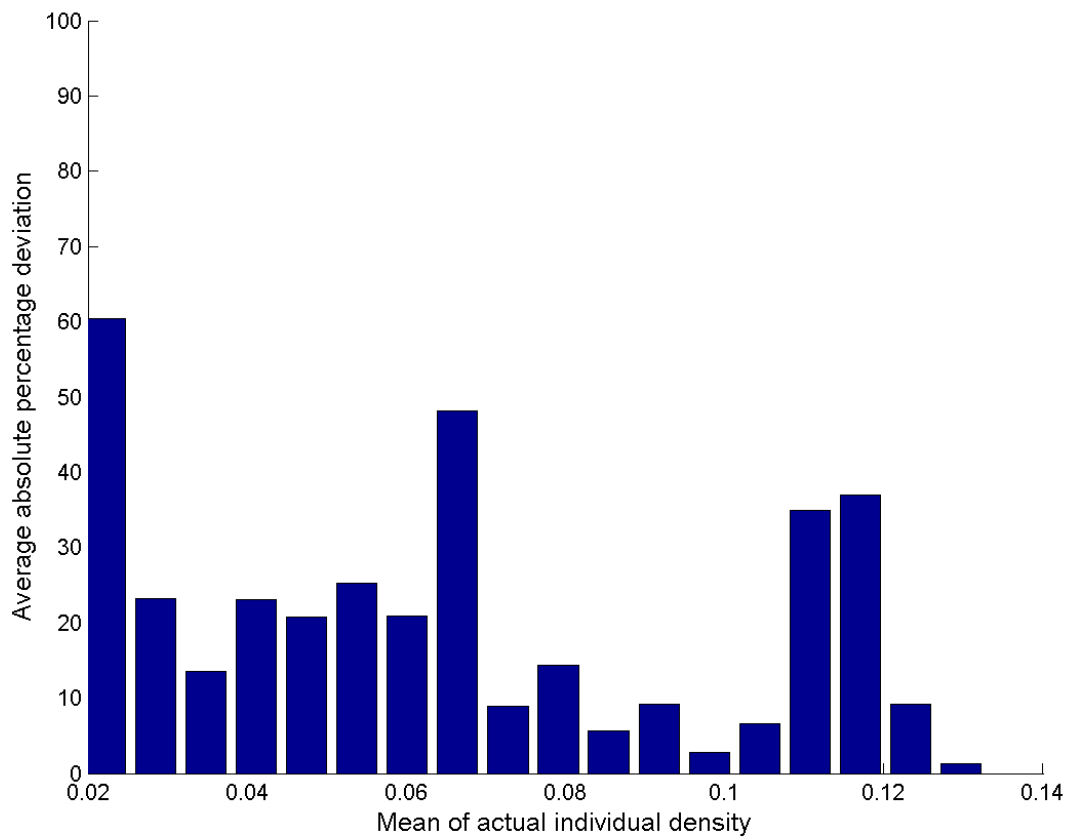


Figure 4.22: Individual Density vs. Average Absolute Percentage Deviation with 0dBm Transmission Power.

Figure 4.22 shows the average absolute percentage deviation (AAPD) from actual density. The results of the AAPD show that the accuracy of the cooperative density estimator is more lower that the previous result in the experiment in -17 dBm transmission power. The average of the AAPD is about 10%. After several attempts the estimating node selected as 232 which be seen in Figure 4.2. This result show us individual density estimation may produce better results depending on the estimating node. Choosing a node closer to the center of the topology, produces a better estimate since the border effect problem is less severe.

4.5 Comparing Individual and Cooperative Density Estimation

Experimental results shows that the performance of the cooperative density estimation is more consistent than individual density estimation. Individual density estimation depends on the position of the estimating node and distribution of its neighbours. When the estimator node resides somewhere close to the middle of the deployment area, the AAPD is low. If a node close to the borders is selected as the estimating node, then the accuracy of the density estimator drops sharply because of the border effect. It can be seen that the individual estimator over-estimates, the cooperative density estimator under-estimates. If these two methods are combined, the accuracy of the new estimator can produce better results.

4.6 Impact of Path-Loss Exponent

Table 4.4: Changes on Individual and Cooperative Estimators According to Path-loss Exponent

γ	λ_c	$\hat{\lambda}_c$	$\sigma_{\hat{\lambda}_c}$	λ_i	$\hat{\lambda}_i$	$\sigma_{\hat{\lambda}_i}$
1.60	0.056	0.006	0.003	0.093	0.031	0.000
2.00	0.056	0.030	0.015	0.078	0.065	0.075
2.50	0.056	0.082	0.016	0.079	0.101	0.000
3.00	0.053	0.166	0.020	0.068	0.444	0.116
3.50	0.055	0.289	0.015	0.079	0.410	0.000

Individual and cooperative density estimation requires a robust path-loss exponent estimator. The error in path-loss exponent estimate significantly impacts the accuracy of the density estimator as can be observed in Table 4.4. The estimated path-loss exponent is usually around 2.32 in our experiments. If we set the path-loss exponent to some values in this range, the error of density estimation -both in individual and cooperative- is smaller compared to those cases where the path-loss exponent largely deviates from the estimated value.

4.7 A New Method Based on Fusion of the Individual and Cooperative Density Estimators

Considering the results of the individual and cooperative density estimation we observed that if a method based on the fusion of these two estimators is performed, then the performance of this new method is much better than these two estimators. It can be understood from the experimental results that while the individual estimator overestimates, the cooperative density estimator underestimates. When we use the average results of these two estimators then the results of estimated and actual density are very close.

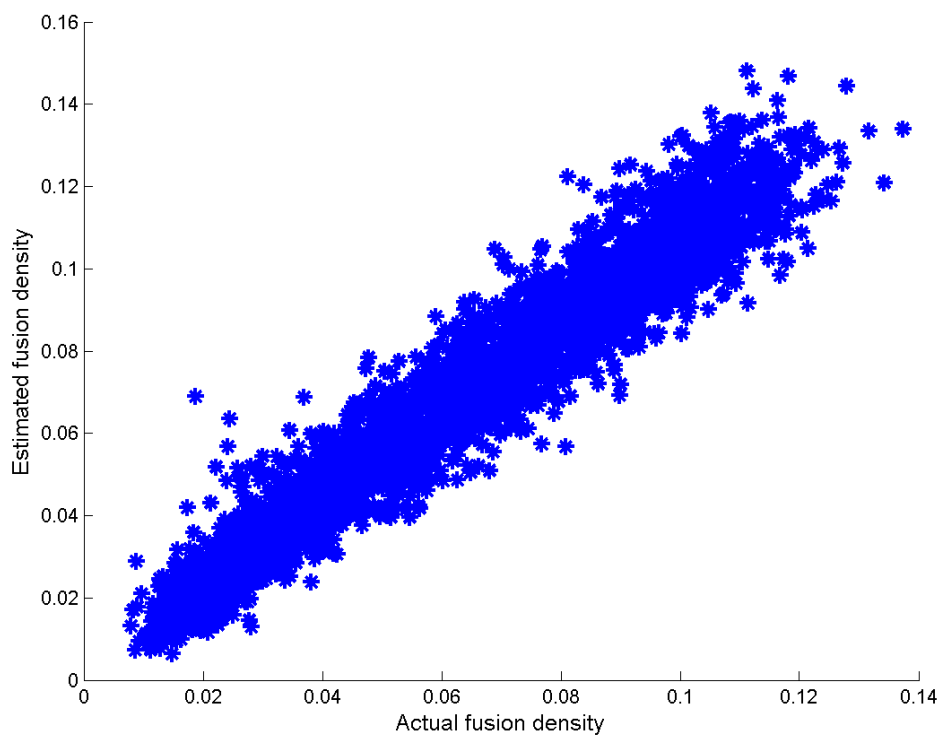


Figure 4.23: Actual Fusion Density vs. Estimated Fusion Density Scatter Plot when Transmission Power is -17 dBm.

Actual fusion density versus the estimated fusion density when the transmission power is -17 dBm is shown in Figure 4.23. As it was the case when the transmission power was -17 dBm, the individual density estimator has overestimated results, and the cooperative density estimator has underestimated outcomes.

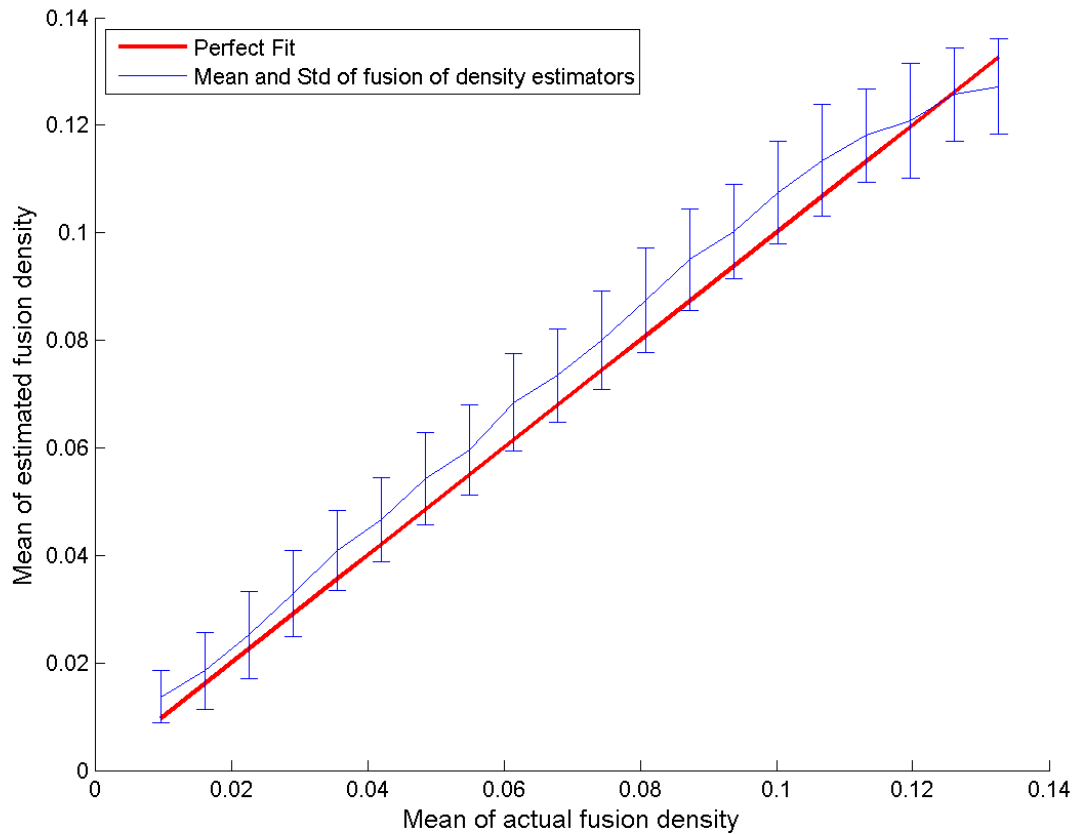


Figure 4.24: Actual Fusion Density vs. Estimated Fusion Density Error Bar when Transmission Power is -17 dBm.

The outcomes are presented with the 95% confidence interval in Figure 4.24 when the transmission power is -17 dBm. In this experiment, the maximum number of nodes is 100. At each run, the density estimator randomly selects 5 nodes in initial step, and 100 nodes at the end. Since we select different nodes at each run, the actual density and the estimated density values change. To present the results, we divide the density range into bins and accumulate the results for each bin. After, we calculate the average of the two estimators, the estimated densities for each bin is averaged and presented in Figure 4.24.

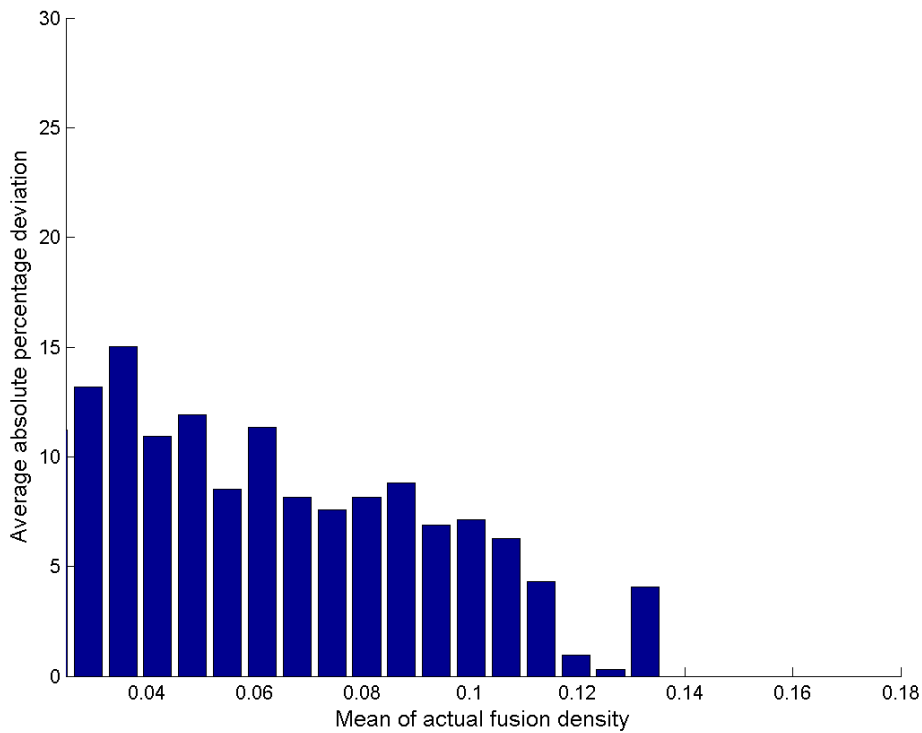


Figure 4.25: Fusion Density vs. Average Absolute Percentage Deviation when Transmission Power is -17 dBm.

The results are shown in terms of average absolute percentage deviation (AAPD) from actual density in Figure 4.25. The results of the AAPD show that the accuracy of the fused density estimator is more accurate than the previous results of the individual and cooperative density estimators when the transmission power is -17 dBm. In this experiment the estimating node in the individual density estimator is again selected as 232 which be seen in Figure 4.2. It can be seen that as the number of nodes increases, the accuracy of the estimator gets much better. The average of the AAPD is about 4%. This result show us the fused density estimation method can produce much better results.

CHAPTER 5

CONCLUSION

5.1 Conclusion

In this thesis, received signal strength based individual and cooperative density estimators are validated by controlled field experiments conducted in the FIT IoT-LAB test-bed, in France. According to the experimental results, individual and cooperative density estimators are not accurately used for density estimation of wireless sensor networks in practice. The accuracy of the individual density estimator is significantly affected by the position of the estimating node and the number of its neighbours. Cooperative density estimator produces more consistent results than the individual density estimator. Therefore, it can be said that cooperative density estimation is more robust than the other. However, the cooperative density estimator effects negatively due to the correlated data. Experimental results show that the average absolute percentage deviation of the cooperative density estimator is around 10%-20%. Meanwhile, the AAPD deviation of the individual density changes between 10% and 35%. These results can be improved by overcoming shadowing and multi-path fading. By considering the experimental and deployment results, we can see that while the individual estimator over-estimates, the cooperative density estimator under-estimates. It can be observed that if these two method are combined, the accuracy of the new estimator can produce better results. Thus, we define a new method based on the fusion of these two estimators in this thesis. This new estimator uses the average results of the estimators, and yields much better outcomes than the results of these two estimators. The average absolute percentage deviation of this new fusion method is around 1%-4%. In this study, it is also observed that the path-loss exponent estimation is an

important issue since it effects the accuracy of density estimation. Moreover, the received signal strength is prone to large- and small-scale fading, and this phenomenon negatively affects the accuracy of the estimators.

5.2 Future Work

There are some possible problems that need to be solved such as how to overcome large- and small-scale fading. These estimators can be more accurate by considering this issue and correlated data while employing in large-scale but limited-range networks. Some hybrid models can be designed by combining the strengths of the individual and cooperative density estimation methods, and especially in the cooperative density estimation, the nodes can share their distance estimations instead of received signal strength measurements. After improving these estimators, they can be implemented as a network protocol. There is also one possible problem which is the validation of these estimators in mobile wireless sensor network.

REFERENCES

- [1] V. Abhayawardhana, I. Wassell, D. Crosby, M. Sellars, and M. Brown. Comparison of empirical propagation path loss models for fixed wireless access systems. In *Vehicular Technology Conference, 2005. VTC 2005-Spring. 2005 IEEE 61st*, volume 1, pages 73–77 Vol. 1, May 2005.
- [2] N. Ahmad, N. Riaz, and M. Hussain. Ad hoc wireless Sensor Network Architecture for Disaster Survivor Detection. *International Journal of Advanced Science and Technology*, 34:9–16, 2011.
- [3] M. Akpeneye, D. Gauthier, Y. Jiang, and J. Kusterer. Viability of deploying wireless stadium networks, 2003.
- [4] I. F. Akyildiz, W. Su, Y. Sankarasubramaniam, and E. Cayirci. Wireless sensor networks: A survey. *Comput. Netw.*, 38(4):393–422, Mar. 2002.
- [5] J. Bachrach and C. Taylor. *Localization in Sensor Networks*, pages 277–310. John Wiley and Sons, Inc., 2005.
- [6] E. Bulut and I. Korpeoglu. Sleep scheduling with expected common coverage in wireless sensor networks. *Wirel. Netw.*, 17(1):19–40, Jan. 2011.
- [7] D. Carlson and A. Terzis. Flip-mac: A density-adaptive contention-reduction protocol for efficient any-to-one communication. In *Distributed Computing in Sensor Systems and Workshops (DCOSS), 2011 International Conference on*, pages 1–8, June 2011.
- [8] Y.-T. Chen, M.-F. Horng, C.-C. Lo, S.-C. Chu, J.-S. Pan, and B.-Y. Liao. A transmission power optimization with a minimum node degree for energy-efficient wireless sensor networks with full-reachability. *Sensors*, 13(3):3951–3974, 2013.
- [9] S. Chitte, S. Dasgupta, and Z. Ding. Distance estimation from received signal strength under log-normal shadowing: Bias and variance. *Signal Processing Letters, IEEE*, 16(3):216–218, March 2009.
- [10] J.-H. Choi, J.-K. Choi, and S.-J. Yoo. Iterative path-loss exponent estimation-based positioning scheme in wsns. In *Ubiquitous and Future Networks (ICUFN), 2012 Fourth International Conference on*, pages 23–26, July 2012.
- [11] M.-C. Chuah and P. Yang. Performance evaluation of node density-based adaptive routing scheme for disruption tolerant networks, 2006.

- [12] J. Deng, Y. S. Han, P.-N. Chen, and P. Varshney. Optimal transmission range for wireless ad hoc networks based on energy efficiency. *Communications, IEEE Transactions on*, 55(9):1772–1782, Sept 2007.
- [13] V. Garg and M. Jhamb. A Review of Wireless Sensor Network on Localization Techniques. 4(April):1049–1053, 2013.
- [14] S. Gezici. A survey on wireless position estimation. *Wireless Personal Communications*, 44(3):263–282, 2008.
- [15] A. Goldsmith. *Wireless Communications*. Cambridge University Press, 2005.
- [16] P. Gupta, S. Member, and P. R. Kumar. The Capacity of Wireless Networks. *IEEE Transactions On Informattion Theory*, 46(2):388–404, 2000.
- [17] IoT-LAB. Fit iot-lab. <https://www.iot-lab.info/>. Accessed: 2015-01-25.
- [18] IoT-LAB. Fit iot-lab m3 nodes. <https://www.iot-lab.info/hardware/m3/>. Accessed: 2015-01-25.
- [19] J.-C. Kuo, W. Liao, and T.-C. Hou. Impact of node density on throughput and delay scaling in multi-hop wireless networks. *Trans. Wireless. Comm.*, 8(10):5103–5111, Oct. 2009.
- [20] Z. Li, Y. Zhao, Y. Cui, and D. Xiang. A Density Adaptive Routing Protocol for Large-Scale Ad hoc Networks. *IEEE*, pages 2597–2602, 2008.
- [21] A. Loukas. Nest : A Practical Algorithm for Neighborhood Discovery in Dynamic Wireless Networks using Adaptive Beaconing. *Delft Universty of Technology Embedded Software Report Series*, 2012.
- [22] G. Mao, B. D. Anderson, and B. Fidan. Path loss exponent estimation for wireless sensor network localization. *Computer Networks*, 51(10):2467 – 2483, 2007.
- [23] G. Mao, B. Fidan, and B. D. Anderson. Wireless Sensor Network Localization Techniques. *Computer Networks*, 51(10):2529–2553, July 2007.
- [24] M. Mbida and A. Ezzati. RTH-RSS Mac : Path Loss Exponent Estimation with Received Signal Strength Localisation Mechanism in Wireless Sensor Networks. 1(2):1–6, 2014.
- [25] P. Moravek, D. Komosny, M. Simek, M. Jelinek, D. Girbau, and A. Lazaro. Signal Propagation and Distance Estimation in Wireless Sensor Networks. 2010.
- [26] Z. Nadir and M. I. Ahmad. Pathloss Determination Using Okumura-Hata Model And Cubic Regression For Missing Data For Oman. II(1):17–20, 2010.

- [27] M. Nakatsuka, H. Iwatani, and J. Katto. A study on passive crowd density estimation using wireless sensors, 2008.
- [28] E. Navarro-alvarez, M. Siller, and K. O. Keefe. GPS-Assisted Path Loss Exponent Estimation for Positioning in IEEE 802 . 11 Networks. 2013, 2013.
- [29] E. Onur, Y. Durmus, and I. Niemegeers. Cooperative Density Estimation in Random Wireless Ad Hoc Networks. *IEEE Communications Letters*, 16(3):331–333, Mar. 2012.
- [30] J. H. Pollard. On Distance Estimators of Density in Randomly Distributed Forests, 1971.
- [31] S. I. Popoola and O. F. Oseni. Empirical Path Loss Models for GSM Network Deployment in. 3(6):85–94, 2014.
- [32] J. G. Proakis. *Digital Communications*. Mc Graw Hill, 4nd edition, 2000.
- [33] C. C. Pu, S. Y. Lim, and P. C. Ooi. Measurement arrangement for the estimation of path loss exponent in wireless sensor network. In *Computing and Convergence Technology (ICCCT), 2012 7th International Conference on*, pages 807–812, Dec 2012.
- [34] N. Rakesh and S. K. Srivatsa. A Study On Path Loss Analysis For Gsm Mobile Networks For Urban , Rural And Suburban Regions Of K Arnataka State. 4(1):53–66, 2013.
- [35] M. V. Ramesh. Design, Development, and Deployment of a Wireless Sensor Network for Detection of Landslides. *Ad Hoc Networks*, 13:2–18, Feb. 2014.
- [36] S. Ranvier. Path loss models. (November), 2004.
- [37] T. Rappaport. *Wireless Communications: Principles and Practice*. Prentice Hall PTR, Upper Saddle River, NJ, USA, 2nd edition, 2001.
- [38] T. Rault, A. Bouabdallah, and Y. Challal. Energy Efficiency in Wireless Sensor Networks: A Top-down Survey. *Computer Networks*, 67:104–122, July 2014.
- [39] M. Raza, L. Hughes, and I. Raza. Density: A context parameter of ad hoc networks. In O. Castillo, L. Xu, and S.-I. Ao, editors, *Trends in Intelligent Systems and Computer Engineering*, volume 6 of *Lecture Notes in Electrical Engineering*, pages 525–540. Springer US, 2008.
- [40] C. Republic. Adaptive Distance Estimation Based on RSSI. pages 1162–1168.
- [41] F. Shen, M.-T. Sun, C. Liu, and A. Salazar. Coverage-aware sleep scheduling for cluster-based sensor networks. In *Proceedings of the 2009 IEEE Conference on Wireless Communications & Networking Conference, WCNC'09*, pages 2480–2485, Piscataway, NJ, USA, 2009. IEEE Press.

- [42] S. Srinivasa and M. Haenggi. Path Loss Exponent Estimation in Large Wireless Networks. 2009.
- [43] R. Stoleru, T. He, J. A. Stankovic, and D. Luebke. A High-Accuracy , Low-Cost Localization System for Wireless Sensor Networks. pages 13–26, 2005.
- [44] J. Walsh, S. Ramanan, and P. Regalia. Optimality of expectation propagation based distributed estimation for wireless sensor network initialization. In *Signal Processing Advances in Wireless Communications, 2008. SPAWC 2008. IEEE 9th Workshop on*, pages 620–624, July 2008.
- [45] K. Whitehouse, C. Karlof, and D. Culler. A practical evaluation of radio signal strength for ranging-based localization. *ACM Mobile Computing and Communications Review (MC2R), Special Issue on Localization Technologies and Algorithms*, 2006.
- [46] Y. Xu and W.-c. Lee. PSGR : Priority-based Stateless Geo-Routing in Highly Dynamic Sensor Networks. *IEEE*, pages 1–20, 2008.
- [47] Z. Yang. A survey on localization in wireless sensor networks, 2005.
- [48] Y. Yuan, C. Qiu, W. Xi, and J. Zhao. Crowd density estimation using wireless sensor networks. In *Mobile Ad-hoc and Sensor Networks (MSN), 2011 Seventh International Conference on*, pages 138–145, Dec 2011.
- [49] Q. Zhu, C. Wang, X. Chen, C. Chen, X. Wang, and C. Zhang. Path loss prediction model of radio propagation over lunar surface. In Y. Wu, editor, *High Performance Networking, Computing, and Communication Systems*, volume 163 of *Communications in Computer and Information Science*, pages 556–562. Springer Berlin Heidelberg, 2011.